SYNTHESIS, REACTIVITY AND ELECTROCHEMICAL STUDIES OF INDIUM FERROCENYL COMPOUNDS

By

Maddie Greatorex

A thesis submitted to the

Department of Chemistry and Biochemistry

Mount Allison University

in partial fulfillment of the requirements for the

Bachelor of Science degree with Honours

April 2023

Thesis Committee

Thesis Committee

Supervisor

Dr. Glen Briand
Professor of Chemistry

Reviewer

Dr. Gregory Sandala
Professor of Chemistry

Table of Contents

Thesis Committee……..……...……1

Acknowledgements…….……...…….…….5

List of Figures, Schemes and Tables.……..…7

List of Spectra in Appendix.…….……..9

Glossary of Abbreviations and Symbols ……..…….....10

Abstract……..……..……..……11

1. Introduction…….…….12

1.1 Green Chemistry……..12

1.2 Catalysis……..……..14

1.3 Indium and Indium Catalysts…….…….……16

1.4 Ferrocenyl Ligands……..…….……18

1.5 Synthesis of Monolithioferrocene……..…….…….19

1.6 Current Study……..…….20

2. Experimental...……..22

2.1 General Methods……..……22

2.1.1 Instrumentation…….……..22

2.1.2 Reagents……...……22

2.2 Attempted One-Pot Synthesis of $InFc_2Cl$…….…….…….22

2.3 Synthesis of FcLi…….……..23

2.4 Synthesis of $InFcCl_2(py)_2$ (1).……...23

2.5 Synthesis of $In_3Fc_4Cl_3O(py)_2$ (2)…..……..24

2.6 Chemical Oxidation of 1-2……...……...…25

2.6.1 Reactivity of $InFcCl_2(py)_2$ (1) with I_2…….…….……..25

2.6.2 Reactivity of $In_3Fc_4Cl_3O(py)_2$ (2) with I_2……25

2.7 X-Ray Crystallography…….…….…….……26

2.8 Computational Studies……..……..…..27

2.9 Electrochemical Studies……..……..……28

3. Results & Discussion……...….29

3.1 Attempted One-Pot Synthesis of $InFc_2Cl$…….……...…29

3.2 Synthesis of FcLi……..…….30

3.3 Attempted Synthesis of $InFc_2Cl$…….……...……...32

3.3.1 Synthesis of $InFcCl_2(py)_2$ (1)……...32

3.3.2 Synthesis of $In_3Fc_4Cl_3O(py)_2$ (2)…….35

3.3.3 Attempted Synthesis of $InFc_2Cl$……..39

3.4 Reactivity and Computational Studies of Complexes 1 and 2…….....40

3.4.1 Reactivity of $InFcCl_2(py)_2$ with I_2…….....…...40

3.4.2 Reactivity of $In_3Fc_4Cl_3O(py)_2$ with I_2……...…....…….……..42

3.5 Electrochemical Studies of Complexes 1 and 2……..…..……44

4. Conclusions……..……47

5. Future Directions…….……48

6. References……...……..49

7. Appendix……..52

Acknowledgements

I'd like to express my sincere appreciation to the people who made this work possible, without whom I would not have able to complete my research or have written my thesis. First, I would like to express my deepest gratitude to Dr. Glen Briand for the opportunity to complete this research under his supervision. I truly appreciate his enthusiasm and the support he has offered me throughout the four years I've spent at Mount Allison. The guidance and expertise he has offered throughout my research has been invaluable. Secondly, I'd like to extend my sincere thanks to my second reader Dr Gregory Sandala. Dr. Sandala has taught me the importance of effective scientific writing and thinking critically. This endeavour would not have been possible without my thesis committee; thank you for providing your knowledge and time to assist me in my research efforts. I am extremely grateful for the generous funding from the Dr. L.A. Goodridge Endowment, which allowed me to complete this research.

I would like to extend my acknowledgement to the entire Department of Chemistry and Biochemistry at Mount Allison. To Susan, Eva, and all my TAs, thank you for teaching me the necessary laboratory techniques to complete this research. To Dan, thank you for always being approachable and friendly, and training me in the use of the NMR spectrometer. To Phil, thank you for teaching me how to work in a laboratory safely and for your patience. To Dr. Megan Roberts, thank you for allowing me to complete an independent study to expand my research capabilities.

Finally, I am eternally grateful to my family and close friends for their support. None of this would've been possible without their kind words and encouragement. I'd also like to thank the

family I've gained here at Mount A—Meagan, Sophie, Torrie, Hilary and Lauren—for their unwavering moral support. Lastly, I'd like to thank the Metal Heads—Padma, Grace, and John—for all the fun times we've had together in lab. An extra thank you to Padma for the computational contribution to this research. I look forward to hearing about all your successes in the future. Thank you for taking the time to read my thesis!

List of Figures, Schemes and Tables

Figure 1. The Twelve Principles of Green Chemistry, as established by Anastas and Warner.[4]

Figure 2. The catalytic two-electron redox cycle of Wilkinson's Catalyst.

Figure 3. A typical three-coordinate indium (III) species with an empty p-orbital.[16]

Figure 4. Reversible one-electron oxidation of ferrocene ligand (Fc) to ferrocenium ion (Fc^+).

Figure 5. (1) General structure of ferrocenophane in the anti-conformation [E= Al, Ga or In]. (2) A synthesized indium-bridged ferrocenophane prepared by Luca and Crabtree.[27]

Figure 6. The target indium complex ($InFc_2Cl$).

Figure 7. X-ray crystal structure of **1** where all hydrogens are removed for clarity. C(1)-In(1)-Cl(2) = 127.53(8), C(1)-In(1)-N(1) = 90.84(11), C(1)-In(1)-N(2) = 93.82(11).

Figure 8. X-ray crystal structure of **2** where all hydrogens are omitted for clarity.

Figure 9. X-ray crystal structure of the core of **2** with only pyridine N atoms and ferrocenyl α-C atoms shown for clarity.

Figure 10. The calculated HOMO of complex **1** where all hydrogens are omitted for clarity.

Figure 11. The calculated HOMO of complex **2** where all hydrogens are omitted for clarity.

Figure 12. Cyclic voltammogram for compound **1** (1 mM in CH_3CN/0.1 M Bu_4NPF_6, platinum disk electrode, 100 mV/sec).

Figure 13. Cyclic voltammogram for compound **2** (1 mM in CH_3CN/0.1 M Bu_4NPF_6, platinum disk electrode, 100 mV/sec).

Scheme 1. One-pot synthesis of the target $InFc_2Cl$ complex via t-butyllithium and subsequent salt elimination using indium trichloride.

Scheme 2. Synthesis and isolation of the FcLi intermediate via the addition of tBuLi to ferrocene,[28] followed by a subsequent salt elimination reaction with indium trichloride and pyridine in THF.

Scheme 3. Improved synthesis of monolithioferrocene intermediate via the addition of tBuLi to ferrocene, with subsequent addition of n-hexane.

Scheme 4. Proposed synthesis of $InFc_2(py)_2Cl$ via a salt elimination reaction.

Scheme 5. Proposed synthesis of $InFc_2(py)Cl$ via a salt elimination reaction.

Scheme 6. Proposed synthesis of $InFc_2Cl$ via a salt elimination reaction.

Scheme 7. Addition of **1** to a solution of I_2 in THF to afford the predicted product $InFcCl_2I$.

Scheme 8. Addition of complex **2** to a solution of I_2 in THF to afford the predicted product $In_3Fc_4Cl_3O(py)$.

Table 1. Crystallographic data for $InFcCl_2(py)_2$ **(1)** and $In_3Fc_4Cl_3O(py)_2$ **(2)**.

List of Spectra in Appendix

Figure A.1: ^{1}H-NMR spectrum in $CDCl_3$ of the product from the reaction of 2 Fc + 2 tBuLi + $InCl_3$.

Figure A.2: ^{1}H-NMR spectrum in $CDCl_3$ of $InFcCl_2(py)_2$ **(1).**

Figure A.3: $^{13}C\{^{1}H\}$-NMR spectrum in $CDCl_3$ of $InFcCl_2(py)_2$ **(1).**

Figure A.4: FT-IR spectrum of $InFcCl_2(py)_2$ **(1).**

Figure A.5: ^{1}H-NMR spectrum in $CDCl_3$ of $In_3Fc_4Cl_3O(py)_2$ **(2)**.

Figure A.6: $^{13}C\{^{1}H\}$-NMR spectrum in $CDCl_3$ of $In_3Fc_4Cl_3O(py)_2$ **(2)**.

Figure A.7: FT-IR spectrum of $In_3Fc_4Cl_3O(py)_2$ **(2)**.

Figure A.8: ^{1}H-NMR spectrum in $CDCl_3$ of $InFcCl_2(py)_2$ **(1)** reaction with I_2.

Figure A.9: ^{1}H-NMR spectrum in $CDCl_3$ of $In_3Fc_4Cl_3O(py)_2$ **(2)** reaction with I_2.

Figure A.10: ^{1}H-NMR spectrum in $CDCl_3$ of the product from the reaction of 2 Fc + 2 tBuLi + $InCl_3$.

Figure A.11: FT-IR spectra of ferrocene.

Figure A.12: FT-IR spectrum of the product from the reaction of 2 Fc + tBuLi + $InCl_3$.

Figure A.13: ^{1}H-NMR spectrum of the product from the reaction of $InCl_3$ + 2 FcLi.

Glossary of Abbreviations and Symbols

Symbol	Definition
Fc	Ferrocene 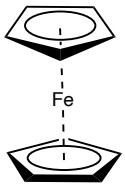
FcLi	Monolithioferrocene 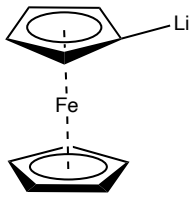
t-Bu	*tert*-butyl
py	Pyridine
THF	Tetrahydrofuran
DCM	Dichloromethane
Et_2O	Diethyl ether
$CDCl_3$	Deuterated Chloroform
M	Molarity (mol/L)
mL	Millilitre
mmol	Millimole
NMR	Nuclear Magnetic Resonance
ppm	Parts per million

Symbol	Definition
s	Singlet
m	Multiplet
CV	Cyclic Voltammetry

Abstract

The sustainability of ‘Green Chemistry’ has led to its widespread adoption in many chemical processes. Of the twelve principles of Green Chemistry, catalysis is the ninth principle and promotes the use of catalytic reagents in place of traditional stoichiometric reagents to significantly reduce waste generation. Precious transition metal complexes are frequently used in catalysis because of their favourable redox properties. But such metals are relatively toxic, expensive, and have a low abundance. By comparison, indium has been explored as a potential alternative because of its low toxicity and high stability. However, indium is stable primarily in the +3 oxidation state and requires the use of a redox-active ligand to impart redox activity. Ferrocene is a redox-active ligand that exhibits a well-defined one-electron reversible redox process. The current study involves the synthesis and characterization of indium complexes containing redox-active ferrocenyl ligands for use as potential green alternatives to transition metal complexes. To this end, the chemical and electrochemical oxidation of these compounds is explored.

1. Introduction

1.1 Green Chemistry

By 1990, the consequences of industrial chemistry and chemical waste were apparent. The Bhopal gas tragedy, an industrial disaster where 45 tons of methyl isocyanate gas escaped a pesticide plant in central India, resulted in the death of more than 15,000 people and more than half a million people were exposed to the gas.[1] This chemical accident sparked political pressure on the chemical industry to integrate new environmental protection measures into process designs.[2] The declaration of the Pollution Prevention Act as a U.S. federal law promoted the reduction or prevention of pollution wherever possible. In the chemical industry, this law stimulated design improvements to reduce the generation of hazardous substances, as opposed to pushing for new methods for treating and disposing of chemical waste. This new approach to chemistry became known as 'Green Chemistry' and was adopted internationally because of its emphasis on molecular sustainability.[3] There are Twelve Principles of Green Chemistry, shown in Figure 1, which are used as guidelines for sustainable design.

12 Principles of Green Chemistry

1. Prevention	7. Use of Renewable Feedstocks
2. Atom Economy	8. Reduce Derivatives
3. Less Hazardous Chemical Synthesis	9. Catalysis
4. Designing Safer Chemicals	10. Design for Degradation
5. Safer Solvents and Auxiliaries	11. Real-Time Analysis for Pollution Prevention
6. Design for Energy Efficiency	12. Inherently Safer Chemistry for Accident Prevention

Figure 1. The Twelve Principles of Green Chemistry, as established by Anastas and Warner.[4]

These twelve principles promote the importance of minimizing hazardous conditions and reducing the risk of accidents and damage by designing safer and sustainable chemicals and processes.[4] Ideally, all twelve principles will be applied when designing chemical transformations. While it is rarely possible to apply each principle in a given synthesis, the use of any Green Chemistry principle is beneficial.

The adoption of Green Chemistry and its principles has led to the modification of many industrial processes. For example, the synthetic procedure of the phosphodiesterase (V) inhibitor sildenafil citrate (Viagra) was improved substantially by incorporating several Green Chemistry principles. For example, the Pfizer UK laboratories initially obtained an abysmal 4.2% overall yield for a linear eleven-step synthesis for the synthesis of the pharmaceutical starting from 2-pentanone.[5] This synthetic route also required the use of various noxious compounds. This, along with the extremely low yields and the generation of hazardous chemicals, limited the application of this reaction in large scale manufacturing. Using the principles of Green Chemistry, the synthetic process was thus redesigned to reduce the large amounts of toxic waste that were being generated. A convergent synthesis was proposed where the advanced intermediates of the reaction were simultaneously prepared and purged from impurities.[5] This redesign also radically reduced the amount of solvent used from 1300 L/kg to only 7 L/kg and it produced just a quarter of the waste than produced in the original process.[6] Green solvents, such as water, t-butanol and ethyl acetate, were introduced in place of ether and toxic chlorinated solvents. The overall yield of the reaction was significantly improved, too, with the average yield of the last three synthetic steps increased to 97%.[5] This new process was able to reduce the amount of hazardous waste generated and the amount of solvent used, all while maximizing the overall yield of synthesized Viagra.

In another example, the industrial synthesis of LY300164, a potential therapeutic agent for the treatment of neurodegenerative disorders such as Alzheimer's and Huntington's disease, was also modified to align with the principles of Green Chemistry.[5] The original eight-step synthesis provided an overall yield of 22% and required use of the hazardous chemicals chromium (III) trioxide, perchloric acid, borane and hydrazine.[5] The metal oxidation reaction produced 3 kg of chromium waste per kilogram of product. These high levels of toxic waste prompted the development of a new synthetic process for more environmentally benign protocols and to reduce the amount of waste generated. The required chirality of LY300164 was introduced at the beginning of the synthetic route, tripling the overall yield.[5] This was accomplished through a biocatalytic reduction where an enzyme is used to catalyze a reduction reaction with high levels of stereo-chemoselectivity.[7] The oxidation step at the benzylic center was accomplished by air via a base-mediated oxidation, instead of the chromium oxidant, allowing for a significant reduction in the amount of hazardous chromium waste produced. There was also a strong motivation to remove carcinogenic hydrazine from the synthetic process, which was achieved through catalytic hydrogenation in ethanol using potassium formate as the hydrogen source rather than hydrazine.[5] In redesigning the original synthetic process, fewer steps were required. Notably, the introduction of a catalyst reduced the number of reagents required and the amount of waste generated. Catalytic reagents, as the ninth principle of Green Chemistry, are highly beneficial throughout chemistry, with catalysis being a main incentive for this project.

1.2 Catalysis

A common method to minimize or eliminate waste in the manufacturing of chemicals is catalysis. Catalysis has been implemented into 90% of all industrial chemicals produced

worldwide enabling energy and resource efficient chemical transformations.[8] The use of stoichiometric reagents in synthetic reactions is automatically associated with waste production, like CrO_3 in LY300164 synthesis.[5] Catalytic reagents are therefore superior to stoichiometric reagents.[8] A catalyst is a substance that accelerates a reaction without itself being consumed in the process.[4] A catalyst decreases the activation energy required for a chemical reaction, increases the rate of the reaction and achieves high selectivity, all without being consumed.[8] This allows for catalysts to be recycled indefinitely without generating waste.[9] Catalysis offers numerous advantages to the field of Green Chemistry, such as reduced amounts of reagents required in syntheses, fewer separation processes, decreased use of toxic materials and increased reaction selectivity.[10]

Precious transition metal catalysts have been used extensively in modern organic and organometallic chemistry because of their variable oxidation states and coordination numbers, their ability to form complex ions and their catalytic activity.[11] Transition metals can readily bond with almost every other element and most organic molecules and moieties. The ligands coordinated to the transition metal centers are able to influence the catalytic activity by modifying the steric or electronic environment of the active site.[12]

A catalytic cycle for a transition metal catalyst is a multistep reaction mechanism often consisting of a series of oxidative addition and reductive elimination reactions. For instance, the catalytic cycle of Wilkinson's catalyst, a coordination complex of rhodium, is widely used in the hydrogenation of alkenes **(Figure 2).**

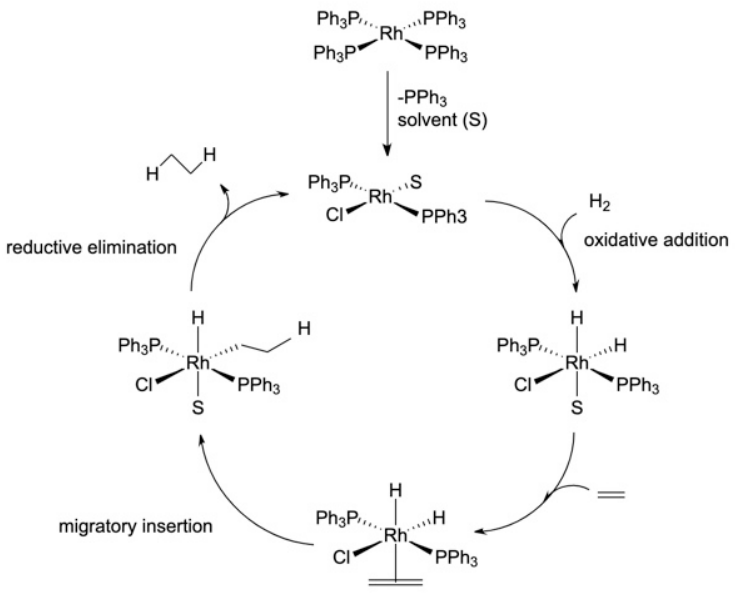

Figure 2. The catalytic two-electron redox cycle of Wilkinson's Catalyst.

The catalytic cycle shown in **Figure 2** is a two-electron transfer process where the rhodium metal centre is oxidized and reduced to complete the hydrogenation reaction. In the past, precious metals have been used extensively in homogenous catalysis for nearly all two-electron transformations as they readily undergo redox reactions.[13] The development of alternative metal catalysts has been of recent interest because of the environmental, health and financial issues associated with precious metal catalysts.[13] Abundant base metals have been explored as alternatives to these scarce elements, often by modifying their reactivities with supporting ligands.[14] In this investigation, indium will be the metal center explored as an alternative to toxic transition metal catalysts because of its low toxicity and cost.[15]

1.3 Indium and Indium Catalysts

Indium (In) is a heavy main group metal that has gained considerable attention as a Lewis acid catalyst in recent years because of the acidic nature of its empty p-orbital. Indium is a Group 13

element with two main oxidation states of +1 and +3, where In(III) is the most stable state. Indium can form bonds using its three valence electrons in the 5s and 5p orbital, and act as an electron acceptor through its vacant low-energy p-orbital (Figure 3).[16] Because of the relatively larger ionic radius of indium(III), it is less reactive as a Lewis acid than boron (III) or aluminum (III). However, this feature allows indium to exhibit a much higher chemoselectivity and higher functional group tolerance.[17] The large size of the indium atom, moreover, allows for high coordination numbers as well as fast coordination–dissociation equilibria when acting as a catalyst.[16]

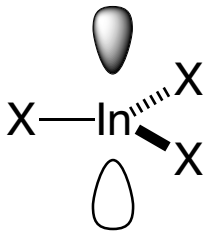

Figure 3. A typical three-coordinate indium (III) species with an empty p-orbital.[16]

Indium (III) reagents are well-established as Lewis acids in a variety of synthesis reactions, such as nucleophilic addition reactions to aldehydes and ketones, Diels-Alder and Friedel-Crafts reactions. In(III) has also been explored as a π-Lewis acid for the activation of unsaturated systems, such as alkynes or alkenes, towards nucleophilic addition[17] and has also been utilized for asymmetric catalysis.[18] A chiral dinuclear indium complex was recently developed as a Lewis acid catalyst for the living ring-opening polymerization of lactide.[19] The wide range of catalytic applications of indium has prompted this research to identify novel indium catalysts to act as transition metal alternatives.

Indium-based catalysts are beneficial to the field of Green Chemistry because of their low toxicity, high functional group tolerance, their use in protic medium and their stability toward air and moisture.[20] However, the lack of accessible redox active states means that indium itself is not

a redox-active metal. Unlike the typical transition metal employed in homogenous catalysts, indium is only stable in the +3-oxidation state, thereby limiting its ability to participate in a catalytic cycle since it is unable to interchange between oxidation states. By comparison, indium can exhibit redox activity and behave as a catalyst when coordinated to appropriate redox-active ligands.

1.4 Ferrocenyl Ligands

Ferrocene has attracted much attention due its high solubility, chemical stability,[21] and unique reversible electrochemical properties **(Figure 4)**. Ferrocene and ferrocenyl ligands have been used as molecular sensors and as catalysts for various chemical reactions.[22] Moreover, ferrocene behaves as the redox-active component in various homo- and heterometallic transition metal complexes.[23] It possesses a fast and reversible one-electron redox reaction between ferrocene and the ferrocenium ion (FcII/FcIII).[22] A well-defined reversible $Fc \rightarrow Fc^{+} + e^{-}$ process is generally observed when both complexes are soluble in the media of interest (Figure 4).[24]

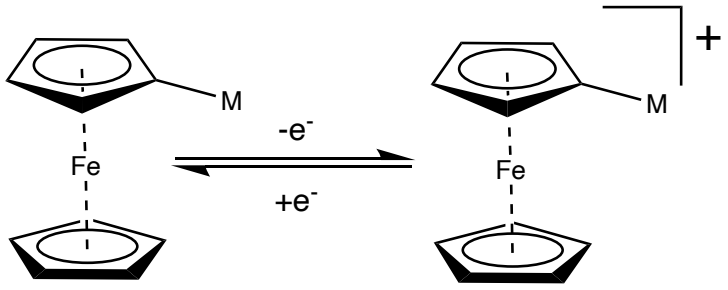

Figure 4. Reversible one-electron oxidation of ferrocene ligand (Fc) to ferrocenium ion (Fc^{+}).

Redox-active ligands facilitate vital multi-electron catalytic reactions and expand the reactivity of various metal complexes.[13,25] These ligands have more energetically accessible energy levels that allow for redox reactions to modify their charge state without changing the oxidation state of

the metal.[14] Hence, the ligand instead becomes the dominant electron source or sink. This property of redox-active ligands has led to an increasing interest in their catalytic applications.[26]

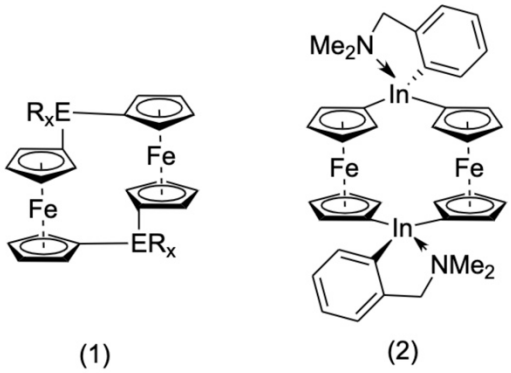

Figure 5. (1) General structure of ferrocenophane in the anti-conformation [E= Al, Ga or In]. (2) A synthesized indium-bridged ferrocenophane prepared by Luca and Crabtree.[27]

Recently, the synthesis and characterisation of an indium-bridged ferrocenophane complex was reported (**Figure 5**). Ferrocenophane is an organometallic derivative of ferrocene that possesses similar electrochemical properties as ferrocene. The redox properties of the indium ferrocenophane complex was examined through cyclic voltammetry (CV).[27] The electrochemical studies performed on the indium ferrocenophane species displayed a conventional stepwise redox cycle.[27] The success of this indium-bridged ferrocenophane prompted the electrochemical investigation of indium compounds of monodentate ferrocenyl ligands.

1.5 Synthesis of Monolithioferrocene

Ferrocene is a common starting material for various chemical processes where it is typically functionalized by electrophilic substitution or metalation.[28] Ferrocene can undergo direct lithiation upon treatment with n-butyllithium (n-BuLi) to obtain mono- and disubstituted ferrocenes.[29]

Monolithioferrocene is an important reagent for metal coordination, yet there is a lack of suitable synthetic routes; direct lithiation of ferrocene by n-BuLi[28], metal–halogen exchange between bromoferrocene and n-BuLi[30] and a transmetallation reaction between chloromercuriferrocene and n-BuLi are the current synthetic routes.[31] A significant drawback of the direct lithiation procedure is the low selectivity as both mono- and dilithiated ferrocene are generated.[29] In addition, these synthetic procedures result in relatively low yields and require the use of toxic materials, and are therefore not viewed as green chemistry processes.

More recently, an optimized high-yield synthesis for large scale (>20 g) preparation of solid monolithioferrocene has been reported.[32] This synthesis was performed via direct lithiation using tert-butyllithium (t-BuLi) to isolate the monolithioferrocene product. This procedure also avoids some common toxic intermediates such as chloromercuriferrocene and ferrocene boronic acid.[32] The success of this reaction procedure prompted its use for a small scale preparation of monolithioferrocene as a reagent in this investigation to synthesize indium ferrocenyl complexes.

1.6 Current Study

The focus of this study is to synthesize and characterize an indium complex containing redox-active ferrocene ligands for use as alternative green catalysts (Figure 6). The target compound of this research contains two ferrocene ligands attached to the indium metal centre to allow for a reversible two-electron oxidation.

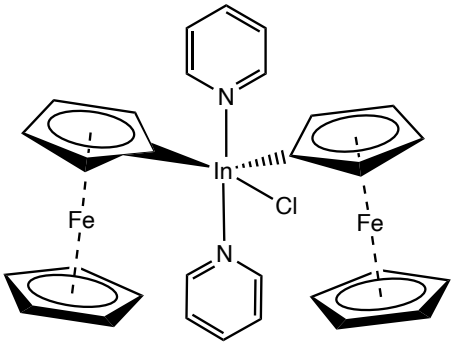

Figure 6. The target indium complex ($InFc_2Cl$).

Pyridine will also be added to the reaction mixture as a monodentate ligand during synthesis to increase the solubility of the target compound and facilitate its crystallization. The indium complexes will be characterized using ^{1}H NMR, $^{13}C\{^{1}H\}$ NMR, FT-IR spectroscopy, melting point, elemental analysis, and X-ray crystallography. Upon successful synthesis of $InFc_2Cl$, its redox properties will be explored using cyclic voltammetry. Finally, reactivity of the indium ferrocenyl complex with the mild oxidants diiodine will be explored.

2. Experimental

2.1 General Methods

2.1.1 Instrumentation

All reactions were carried out under a dinitrogen atmosphere using standard Schlenk line techniques and an Innovative Technology glovebox. Melting points were measured using an Electrothermal MEL-TEMP instrument. ^{1}H and $^{13}C\{^{1}H\}$ NMR spectra were obtained using a Varian Mercury 200 MHz+ spectrometer at 25 °C. The frequencies for ^{1}H NMR and $^{13}C\{^{1}H\}$ NMR were 200 MHz and 50.3 MHz, respectively. FT-IR spectra were obtained using a Thermo Scientific Nicolet iS5 spectrometer. Single-crystal X-ray crystallography was performed by Dr. Jason Masuda at Saint Mary's University. Elemental analysis was performed by Guelph Chemical Laboratories Inc.

2.1.2 Reagents

Ferrocene anhydrous powder (98 %) and indium(III) chloride anhydrous powder (98 %) and tert-butyllithium in pentane (1.7 M) were obtained from Sigma Aldrich and used as received. T-Butyllithium in pentane solution (1.8M) was used as received from Thermo Scientific. Anhydrous toluene (99.8%) and Anhydrous tetrahydrofuran (≥99.9%, inhibitor-free) were obtained from Sigma Aldrich and both were dried using molecular sieves.

2.2 Attempted One-Pot Synthesis of $InFc_2Cl$

A solution of ferrocene (0.286 g, 1.537 mmol) in THF (5 mL) was cooled to -20 °C in an ice-methanol bath. A pentane solution of t-BuLi (0.904 mL, 1.7 M, 1.537 mmol) was added dropwise

over a period of 15 minutes before the reaction was stirred at room temperature for 30 min. This solution was added dropwise to a cloudy white solution of $InCl_3$ (0.170 g, 0.769 mmol) and pyridine (0.122g, 1.537 mmol) in THF (4 mL) that was cooled to -20 °C in an ice-methanol bath. This gave a cloudy yellow-orange solution that was left to stir for 3 h, resulting in a clear amber solution. The solvent was removed under vacuum and the resulting product was redissolved in toluene (6 mL). The solution was filtered and then concentrated to 4 mL and stored at -15 °C. This reaction yielded a crystalline orange product that was confirmed to be ferrocene by ^{1}H NMR. ^{1}H NMR (ppm, $CDCl_3$): 4.16 (s, 10H, CH); **(Figure A.1)**.

2.3 Synthesis of FcLi[32]

A clear, amber solution of ferrocene (4.000 g, 21.501 mmol) in THF (25 mL) was cooled in an ice bath to 0°C. A pentane solution of t-BuLi (14.6 mL, 1.7 M, 24.7 mmol) was added dropwise over a period of 15 min, resulting in a dark red solution. Immediately following the dropwise addition, n-hexane (30 mL) was added, and the mixture was cooled to -78 °C to precipitate the crude product. The orange solution was decanted, and the bright red crude product was washed with n-hexane (5 x 5 mL) until almost colorless. The yellow-orange product FcLi was dried in vacuo and stored at -15 °C. No analytical or spectroscopic data was obtained because of the extreme air-sensitivity of the product. Yield: 1.521 g, 7.841 mmol, 37%.

2.4 Synthesis of $InFcCl_2(py)_2$ (1)

A clear, pale orange solution of FcLi (0.268 g, 1.382 mmol) in THF (6 mL) was cooled to -78 °C and added dropwise to a cloudy, white solution of $InCl_3$ (0.153 g, 0.691 mmol) and pyridine (0.109 g, 1.382 mmol) in THF (4 mL) cooled to -20 °C. This initially resulted in a peach-colored

cloudy solution and was left to stir for 3 h, resulting in a clear, amber solution. The solvent was removed under reduced pressure. The product was redissolved in toluene (5 mL) and the solution was filtered, concentrated to 2 mL, and left at 23 °C for 18 h to afford needle-like crystals of **1**. Yield: 0.071 g, 0.150 mmol, 22%. Elemental Analysis: Calculated: C, 45.41%; H, 3.62%; N, 5.30%. Found: C, 45.55%; H, 3.88%; N, 5.02%. ^{1}H NMR ($CDCl_3$, ppm): 8.62 (m, 4H, NC_6H_5), 7.59 (m, 2H, NC_6H_5), 7.22 (m, 4H, NC_6H_5), 3.84–4.03 (m, 9H, C_5H_5/C_5H_4); **(Figure A.2).** ^{13}C{^{1}H} NMR ($CDCl_3$, ppm): 68.8–72.1 (C_5H_5), 75.6–78.6 (C_5H_4), 77.9 ($CDCl_3$ residue), 125.9 (C3 in pyridine ligand), 126.1 [C(*p*) in toluene residue], 129.2 [C(*m*) in toluene residue], 130.1 [C(*o*) in toluene residue], 139.2 (C4 in pyridine ligand), 139.6 [C(*i*) in toluene residue], 149.8 (C2 in pyridine ligand); **(Figure A.3)**. FT-IR (cm^{-1}): 602 (w), 625 (m), 694 (s), 731 (w), 754 (m), 819 (m), 873 (w), 1006 (m), 1026 (w), 1037 (w-m), 1066 (m), 1105 (m), 1135 (w), 1214 (w), 1238 (w), 1378 (w), 1410 (w), 1445 (m), 1484 (w), 1599 (m), 3086 (w); **(Figure A.4)**. Melting point: 128–134 °C.

2.5 Synthesis of $In_3Fc_4Cl_3O(py)_2$ (2)

A solution of FcLi (0.329 g, 1.70 mmol) in THF (9 mL) was cooled to -78 °C and added dropwise to a solution of $InCl_3$ (0.188 g, 0.848 mmol) and pyridine (0.067 g, 0.848 mmol) in THF (4.5 mL) that was cooled to -20 °C. The solution was left to stir for 3 h, resulting in a clear, burnt orange-coloured solution. The solvent was removed under reduced pressure. The product dissolved in toluene (6 mL), filtered, concentrated to 4 mL, and left to sit at 23 °C for 3 d. This afforded orange block-like crystals of **2.** Yield: 0.17 g, 0.359 mmol, 42%. Elemental Analysis: Calculated: C, 43.99%; H, 3.40%; N, 2.05%. Found: C, 44.17%; H, 3.59%; N, 1.77%. ^{1}H NMR ($CDCl_3$, ppm): 8.62 (m, 4H, NC_6H_5), 7.79 (m, 2H, NC_6H_5), 7.39 (m, 4H, NC_6H_5), 3.86–4.31 (m, 20H, C_5H_5/C_5H_4);

(Figure A.5). $^{13}C\{^{1}H\}$ NMR ($CDCl_3$, ppm): 66.1–69.7 (C_5H_5), 72.9–75.8 (C_5H_4), 74.6 ($CDCl_3$ residue), 123.7 (C3 in pyridine ligand), 138.2 (C4 in pyridine ligand), 146.7 (C2 in pyridine ligand); **(Figure A.6).** FT-IR (cm^{-1}): 412 (m), 439 (s), 569 (m), 603 (s), 636 (s), 657 (s), 694 (s), 754 (s-m), 816 (s), 876 (w), 1000 (m), 1013 (m), 1024 (s), 1042 (s), 1067 (m), 1102 (m), 1135 (m), 1183 (w), 1221 (w), 1296 (w), 1375 (w), 1409 (w-m), 1451 (m), 1489 (w), 1606 (m), 1633 (w), 29267 (w), 3083 (w), 3383 (br); **(Figure A.7)**. Melting point: 182–193 °C.

2.6 Chemical Oxidation of 1-2

2.6.1 Reaction of $InFcCl_2(py)_2$ (1) with I_2

A purple-black solution of I_2 (0.048 g, 0.190 mmol) in THF (1 mL) was added dropwise to a clear, orange solution of $InFcCl_2(py)_2$ (0.201 g, 0.380 mmol) in THF (3 mL). This caused the orange solution to become an opaque dark brown solution. After stirring for 4 h, the solution became a cloudy green-brown colour. The reaction mixture was allowed to settle to give a white precipitate and a dark brown solution. The solution was decanted and allowed to sit at 23 °C for 3 d after which very small colorless needle-like microcrystals had formed. ^{1}H NMR (ppm, $CDCl_3$): 3.83–4.07 (m, 10H, C_5H_5/C_5H_4); **(Figure A.8)**.

2.6.2 Reaction of $In_3Fc_4Cl_3O(py)_2$ (2) with I_2

A purple-black solution of I_2 (0.019 g, 0.0740 mmol) in THF (1 mL) was added dropwise to a cloudy orange solution of $In_3Fc_4Cl_3O(py)_2$ (0.202 g, 0.148 mmol) in THF (5 mL). This caused the orange solution to become an opaque dark brown solution. After 1 h, a solution of I_2 (0.019 g, 0.0740 mmol) in THF (1 mL) was added dropwise and the reaction mixture was stirred for 1 h. This was repeated two more times for a total of 4 molar equivalents of I_2 and a 4 h reaction time.

The resultant green-brown reaction mixture was filtered to remove a small amount of precipitate. The filtrate was concentrated to 5 mL and stored at 23 °C for 3 d after which very small colorless needle-like crystals had formed. ^{1}H NMR (ppm, $CDCl_3$): 8.62 (m, 2H, NC_6H_5), 7.79 (m, 1H, NC_6H_5), 7.39 (m, 2H, NC_6H_5), 3.83–4.11 (m, 40H, C_5H_5/C_5H_4); **(Figure A.9)**.

2.7 X-Ray Crystallography

Crystals of compounds **1**–**2** were mounted from Paratone-N oil on a MiTeGen MicroMount. The data were collected on a Bruker APEX II charge-coupled-device (CCD) diffractometer, with an Oxford 700 Cryocool sample cooling device. The instrument was equipped with graphite-monochromated Mo Kα radiation (λ=0.71073 Å; 30 mA, 50 mV), with MonoCap X-ray source optics. For data collection, four ω-scan frame series were collected with 0.5° wide scans, 5 second frames and 366 frames per series at varying φ angles (φ=0°, 90°, 180°, 270°). Data collection, unit cell refinement, data processing and multi-scan absorption correction were applied using the APEX2, APEX3 or APEX4 software packages. The structures were solved using SHELXT and all non-hydrogen atoms were refined anisotropically with SHELXL using a combination of shelXle and OLEX2 graphical user interfaces. Unless otherwise noted, all hydrogen atom positions were idealized and reside on the atom to which they were attached. The final refinement included anisotropic temperature factors on all non-hydrogen atoms. Details of crystal data, data collection, and structure refinement are listed in Table 1. All figures were generated using Diamond software.

Table 1. Crystallographic data for $InFcCl_2(py)_2$ **(1)** and $In_3Fc_4Cl_3O(py)_2$ **(2)**.

Molecular Formula	**$C_{20}H_{19}Cl_2FeInN_2$**	**$C_{50}H_{46}Cl_3Fe_4In_3N_2O$**
Formula Weight (g/mol)	528.94	1365.10
Crystal System	Triclinic	Orthorhombic
Space Group	P-1	Pbcn
a (Å)	9.4712(6)	15.4858(3)
b (Å)	14.1711(9)	25.0107(5)
c (Å)	16.0459(9)	12.2709(2)
α (deg)	75.792(2)	90
β (deg)	87.900(2)	90
γ (deg)	87.900(2)	90
V ($Å^3$)	2028.9(2)	4752.65(15)
Z	4	4
F (000)	1048.0	2680.0
ρ (g/cm^3)	1.732	1.908
μ (mm^{-1})	2.121	2.824
T (K)	150.00	150.00

2.8 Computational Studies

All density functional theory (DFT) calculations were performed using Gaussian 16 Revision C.01 using the PBE1PBE-GD3BJ/def2-SVP level of theory for all atoms except In, I and Fe, for which Stuttgart electron core pseudo-potentials were employed. Structures obtained by

X-ray crystallography were used as starting points for the geometry optimizations when possible. Dispersion corrections were included in all calculations using the D3 empirical correction of Grimme with Becke-Johnson dampening (GD3BJ). Unless otherwise indicated, relative energies for each reaction were obtained using total energies of each species as electronic energies plus internal thermal energy (E or U) corrections at 298.15 K.

2.9 Electrochemical Studies

Cyclic voltammetry experiments were carried out in a glove box using a PC-interfaced BASi Epsilon Eclipse potentiostat and proprietary software (version 3.0.84). A platinum-disk working electrode (1.6 mm diameter) and platinum wire counter electrode were used in a 10 mL three-neck round bottom flask. Because of the apparent formation of insulating films during oxidation experiments, the working electrode was cleaned between scans to a potential low enough to observe a reductive stripping peak (~ -1.7 V). Potentials were referenced against a reversible ferrocene wave (Fc/Fc^{+}) by subtracting the observed half-wave potential for this couple ($E_{1/2}$ = + 0.081 V) and then converted to potential vs. SCE by adding 0.380 V to this value. Analyte concentrations were 1 mM, the supporting electrolyte was 0.1 M $[NBu_4][PF_6]$ and all experiments were carried out at 23 °C.

3. Results and Discussion

3.1 Attempted One-Pot Synthesis of $InFc_2Cl$

A one-pot synthesis of $InFc_2Cl$ was attempted that involved the combination and adaptation of two literature syntheses of similar complexes outlined by Mueller-Westerhoff *et al*.[33] and Schachner *et al*.[34] **(Scheme 1).** Mueller-Westerhoff outlined a synthetic preparation of a ferrocene aldehyde in which a monolithioferrocene (FcLi) reagent was synthesized *in situ* from the reaction of ferrocene and t-butyllithium in THF at -20°C. This procedure was combined with the synthesis of an indium-bridged ferrocenophane described by Schachner, which had a similar structure to that of our target indium complex $InFc_2Cl$.

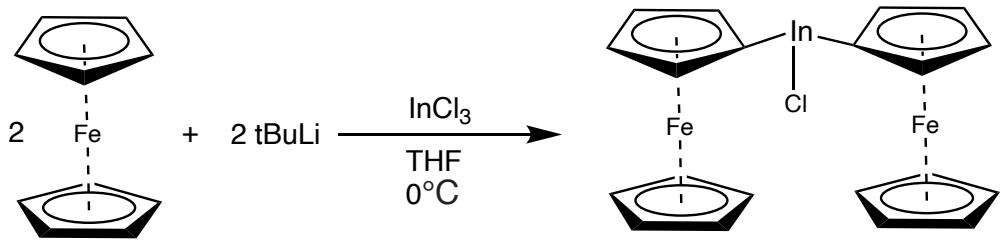

Scheme 1. One-pot synthesis of the target $InFc_2Cl$ complex via t-butyllithium and subsequent salt elimination using indium trichloride.

This procedure afforded block-like orange crystals in good yields. However, the ^1H NMR spectrum of the product was consistent with the reported chemical shifts for ferrocene, showing a strong singlet at 4.16 ppm corresponding to the ten aromatic hydrogens **(Figure A.1)**. The significant amount of unreacted ferrocene starting material indicated that the FcLi intermediate was either not synthesized or was highly unstable in solution. To allow the FcLi intermediate to stabilize *in situ*, the reaction temperature was decreased to -78 °C. Pyridine was also introduced

into the reaction mixture to occupy coordination sites on indium and mimic the previously reported five-coordinate indium-bridged ferrocenophane complex.[34] However, these procedural modifications were unsuccessful as evidenced by the ^{1}H NMR spectra of the product, which remained consistent with that of ferrocene. This indicated that the FcLi intermediate was either not stable enough to react with indium trichloride or was not being synthesized *in situ*. Therefore, it was necessary to evaluate a stepwise synthesis where FcLi was isolated before reaction with $InCl_3$.

3.2 Synthesis of FcLi

The synthetic procedure described by Kagan *et al*[28] was attempted in order to isolate FcLi **(Scheme 2).** This involved the reaction of ferrocene with one equivalent of t-butyllithium at 0 °C. The solution was allowed to warm to 23 °C and the solvent was removed under vacuum to afford FcLi as a red-orange powder. Full characterisation was not completed as FcLi is an extremely air-sensitive pyrophoric material. The lack of characterisation of FcLi was a significant issue during this investigation as the purity of the reagent could not be determined. Instead, a salt elimination reaction of FcLi and indium(III) chloride was completed to assess the reactivity and purity of the FcLi reagent as well as the purity of the final product.

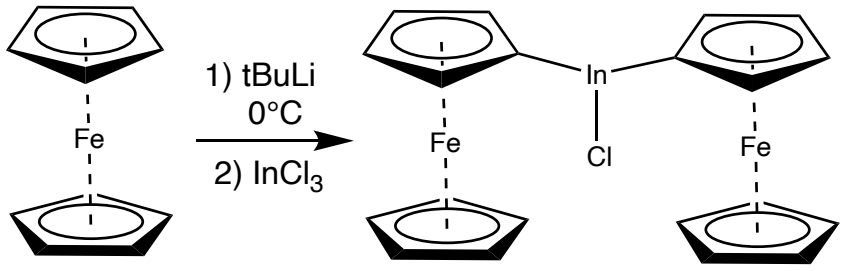

Scheme 2. Synthesis and isolation of the FcLi intermediate via the addition of tBuLi to ferrocene,[28] followed by a subsequent salt elimination reaction with indium trichloride and pyridine in THF.

The ^{1}H NMR spectrum of the product of this reaction displayed a strong singlet at 4.16 ppm **(Figure A.10)**, which is characteristic of ferrocene. However, the FT-IR spectra of the final product was much more complex than that of ferrocene. Broad peaks at 3395 and 2872 cm^{-1} were present in the spectra of the final product, which are not characteristic of ferrocene **(Figure A.11 & Figure A.12)**. There is also evidence of additional stretching frequencies present in the lower wavenumber range; a medium peak at 1023 cm^{-1} corresponds to C-N stretching, suggesting that an indium ferrocenyl complex with pyridine ligands may have been synthesized. In summary, the complete results obtained through ^{1}H NMR and FT-IR spectroscopy are indicative of an impure final product. While the target complex may have been synthesized, high amounts of residual ferrocene present in the final product prevented the ferrocenyl-indium complex from being unequivocally identified and characterized. Melting point determination of both ferrocene and the synthesized indium product were completed, and these results support that a product mixture was present. Because of the presence of impurities as well as low yields of the indium ferrocenyl product, a new procedure for the synthesis of FcLi was attempted, which involved purification of the product before further reaction.

Thus, a large-scale synthesis of FcLi was attempted using t-butyllithium as a base **(Scheme 3).** This process involved the dropwise addition of t-butyllithium to a solution of ferrocene in THF cooled to 0 °C. After addition, the solution was immediately cooled to -80 °C and n-hexane was added to precipitate a bright red crude product, with the solution consisting of a mixture of lithioferrocene and unreacted ferrocene. The reaction precipitate was isolated and washed with portions of n-hexane until the filtrate was colorless, indicating full removal of ferrocene. The product was dried in vacuo to afford a yellow-orange powder of FcLi. This reactive reagent was

stored at -15 °C in a sealed test tube to prevent hydrolysis. Yields of 31–36% were observed each time this procedure was completed. These low yields were somewhat expected due to a 10-fold decrease in reaction scale versus that used in the literature procedure. Again, no analytical or spectroscopic characterisation could be completed because of the extreme air sensitivity of FcLi.

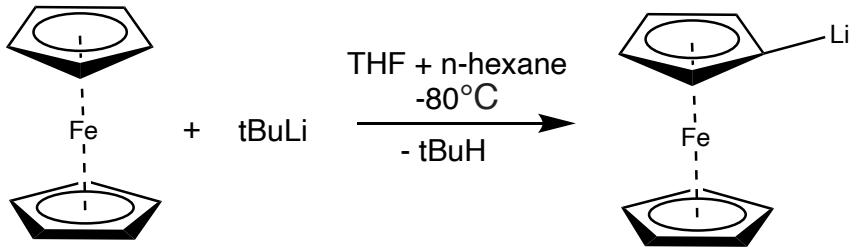

Scheme 3. Improved synthesis of monolithioferrocene intermediate via the addition of tBuLi to ferrocene, with subsequent addition of n-hexane.

3.3 Attempted Synthesis of $InFc_2Cl$

3.3.1 Synthesis of $InFc(py)_2Cl_2$ (1)

A salt elimination reaction of FcLi and indium (III) chloride was carried out at -78 °C in tetrahydrofuran (THF) **(Scheme 4)**. Pyridine was also added with the expectation that it would improve the solubility of $InFc_2Cl$ and fill available coordination sites on the indium metal centre. The reaction was completed in a 2:1:2 stoichiometric ratio of FcLi, $InCl_3$ and pyridine, respectively. The solution was initially yellow-orange and cloudy but became a clear amber solution following the three–hour reaction time. The solution was filtered and concentrated to afford orange needle-like crystals when left in a dinitrogen atmosphere at 23 °C for four days. The crystalline material was then sent for analysis by X-ray crystallography.

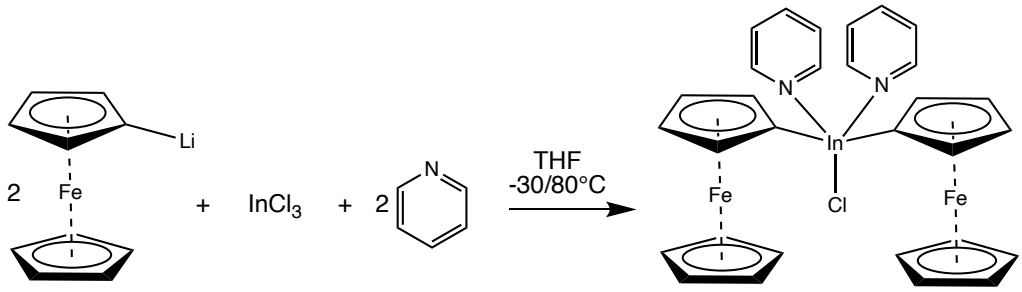

Scheme 4. Proposed synthesis of $InFc_2(py)_2Cl$ via a salt elimination reaction.

However, the X-ray crystallography results showed that while the target molecule $InFc_2(py)_2Cl$ was not synthesized, a novel compound $InFc(py)_2Cl_2$ **(1)** was obtained **(Figure 7)**. The structure of **1** contains two pyridine ligands, two chloride ligand and only one ferrocenyl ligand bound to indium. The structure of **1** shows a monomeric compound and a slightly distorted trigonal bipyramidal bonding environment for indium. Both chloride ligands and a ferrocenyl carbon atom occupy equatorial sites [Cl(2)-In(1)-Cl(1) = 112.97(3)°, C(1)-In(1)-Cl(1) = 119.47(8)°, C(1)-In(1)-Cl(2) = 127.53(8)°] and both pyridine ligands nitrogen atoms occupy axial sites [N(2)-In(1)-N(1) = 175.24(10)].

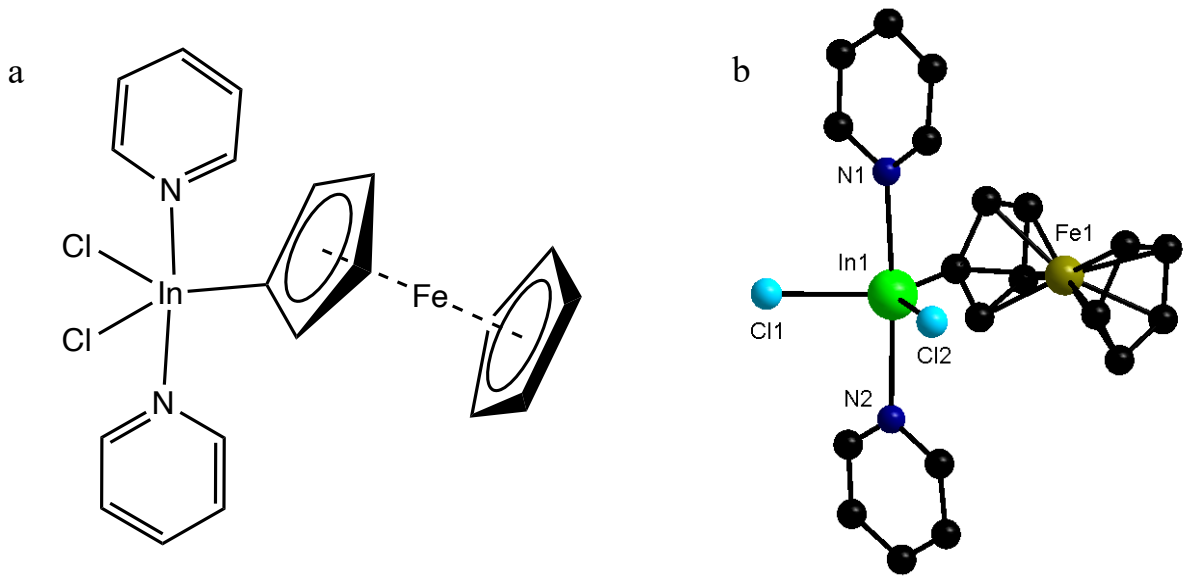

Figure 7. (a) The structure of $InFcCl_2(py)_2$. **(b)** X-ray crystal structure of **1** where all hydrogens are removed for clarity. Selected bond distances (Å) and bond angles (°): In(1)-Cl(1) = 2.4063(8), In(1)-Cl(2) = 2.4053(8), In(1)-N(1) = 2.379(3), In(1)-N(2) = 2.375(3), In(1)-C(1) = 2.129(3), Cl(2)-In(1)-Cl(1) = 112.97(3), N(1)-In(1)-Cl(1) = 88.17(7), N(1)-In(1)-Cl(2) = 88.89(7), N(2)-In(1)-Cl(2) = 88.67(7), N(2)-In(1)-Cl(2) = 89.07(7), N(2)-In(1)-N(1) = 175.24(10), C(1)-In(1)-Cl(1) = 119.47(8), C(1)-In(1)-Cl(2) = 127.53(8), C(1)-In(1)-N(1) = 90.84(11), C(1)-In(1)-N(2) = 93.82(11).

The X-ray crystallography results confirm that only one ferrocenyl ligand was able to bond to indium, presumably because of steric hindrance caused by both axial pyridine ligands, which would prevent the second equivalent of FcLi to react. Therefore, the stoichiometric ratios of the reaction procedure described in Scheme 4 were modified (see Section 3.3.2), with the expectation that both equivalents of ferrocenyl ligand would now bond to indium.

3.3.2 Synthesis of $In_3Fc_4Cl_3O(py)_2$ (2)

The same reaction procedure described in the synthesis of $InFc(py)_2Cl_2$ **(1)** was repeated with the objective of synthesizing the target $InFc_2Cl$ complex. However, the stoichiometric ratios of FcLi, indium(III) chloride and pyridine were modified to be 2:1:1, respectively **(Scheme 5)**. Initially, the reaction provided a cloudy, yellow solution. Following a three–hour stir, the reaction mixture became a clear burnt-orange solution that was filtered and concentrated. This afforded orange block-like crystals in a low crystalline yield when left at 23 °C in a dinitrogen atmosphere for four days. ^{1}H NMR spectroscopy of the product confirmed the expected stoichiometric ratio of ferrocene and pyridine in the isolated complex to be 2:1, and the crystals were sent for X-ray crystallography.

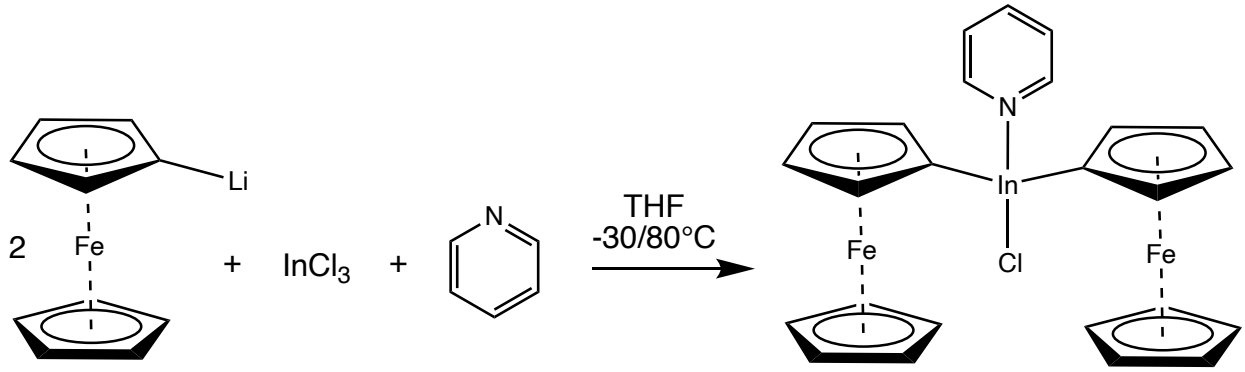

Scheme 5. Proposed synthesis of $InFc_2(py)Cl$ via a salt elimination reaction.

The X-ray crystallography results provided a refined structure of the isolated material that was significantly different than the expected structure **(Figures 8 and 9)**. While $InFc_2Cl(py)$ was not synthesized, these results confirmed the synthesis of $In_3Fc_4(py)_2Cl_3O$ **(2)**, the first trinuclear indium compound with a central oxo (2^-) ligand bridging the three indium(III) centres. This structure was highly unanticipated due the presence of the central oxide ligand. All reactions were completed in a dinitrogen atmosphere and all reagents were stored under dinitrogen. Therefore, it

was believed that water was able to enter the reaction mixture via the FcLi reagent that was stored in a sealed test tube in the freezer to prevent decomposition. It became crucial in the following reactions to minimize freezer storage time of this reactant. While the presence of oxygen in the reaction mixture was unintentional, it was interesting to note that the synthesis of **2** via this method was reproducible, even when different synthetic batches of FcLi were used as the starting material.

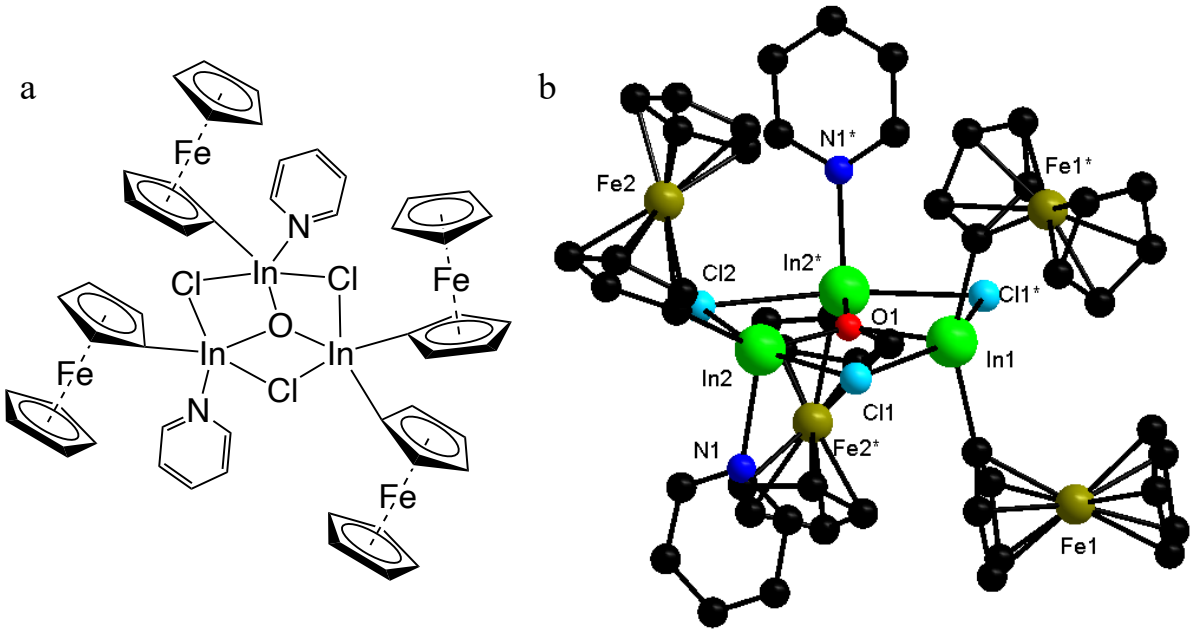

Figure 8. (a) The structure of $In_3Fc_4Cl_3O(py)_2$. **(b)** X-ray crystal structure of **(2)** where all hydrogens are omitted for clarity.

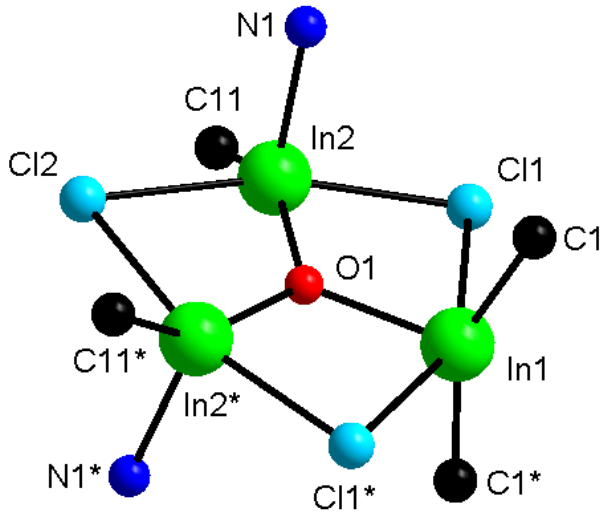

Figure 9. X-ray crystal structure of the core of **2** with only pyridine N atoms and ferrocenyl α-C atoms shown for clarity. Selected bond distances (Å) and bond angles (°) of the complexes' core: In(1)-Cl(1) = 2.8015(4), In(1)-Cl(1*) = 2.8015(4), In(1)-O(1) = 2.1154(16), In(1)-C(1*) = 2.1189(17), In(1)-C(1) = 2.1189(17), In(2)-Cl(1) = 2.5910(4), In(2)-Cl(2) = 2.7544(4), In(2)-O(1) = 2.0152(7), In(2)-N(1) = 2.2594(14), In(2)-C(11) = 2.0963(15), Cl(1*)-In(1)-Cl(1) = 153.098(18), O(1)-In(1)-Cl(1*) = 76.549(9), O(1)-In(1)-Cl(1) = 76.549(9), O(1)-In(1)-C(1*) = 104.04(5), O(1)-In(1)-C(1) = 104.04(5), C(1)-In(1)-Cl(1) = 92.17(5), C(1*)-In(1)-Cl(1) = 94.30(5), C(1*)-In(1)-Cl(1*) = 92.17(5), C(1)-In(1)-Cl(1*) = 94.30(5), C(1*)-In(1)-C(1) = 151.92(9), Cl(1)-In(2)-Cl(2) = 161.132(13), O(1)-In(2)-Cl(1) = 83.36(4), O(1)-In(2)-Cl(2) = 77.83(4), O(1)-In(2)-N(1) = 101.70(4), O(1)-In(2)-C(11) = 147.31(4), N(1)-In(2)-Cl(1) = 93.62(4), N(1)-In(2)-Cl(2) = 91.63(4), C(11)-In(2)-Cl(1) = 99.13(5), C(11)-In(2)-Cl(2) = 95.94(5), C(11)-In(2)-N(1) = 110.60(6).

The structure of **2** shows three indium atoms bridged through a central oxo ligand and three bridging chloride ligands [In(1)-Cl(1) = 2.8015(4), In(2)-Cl(1) = 2.5910(4), In(2)-Cl(2) =

2.7544(4)]. Both In-O bond distances [In(1)-O(1) = 2.1154(16), In(2)-O(1) = 2.0152(7)] were shorter than the average In-O bond distance present in amorphous indium oxide (2.18 Å)[35], which implies that the bridging of indium to oxygen in complex **2** is a very stable bonding interaction.

Two different indium bonding environments were identified in the crystal structure. In(1) is bound to two ferrocenyl ligands while both In(2) centres are bound to one ferrocenyl ligand and one pyridine ligand. In(1) experiences a slightly distorted trigonal bipyramidal geometry. Both chloride atoms occupy axial sites [Cl(1*)-In(1)-Cl(1) = 153.098(18)], whereas the oxo ligand and the ferrocenyl carbon atoms occupy equatorial sites [O(1)-In(1)-C(1) = 104.04(5), C(1*)-In(1)-C(1) = 151.92(9)]. The axial bond angle appears to be contracted as the chloride atom is bridged between two indium centres, prompting both chloride atoms to be pulled slightly inwards within the molecule. The large structural distortion observed between the equatorial sites is most likely due to the large steric hindrance of both ferrocenyl ligands. The C(1*)-In(1)-C(1) bond angle of 151.92° is much larger than the ideal 120°, which is due to the relatively large size of both ferrocenyl ligands.

A distorted trigonal bipyramidal geometry is also observed at the In(2) atom. The ferrocenyl carbon, the bridging oxygen atom and the pyridine nitrogen atom occupy equatorial sites [O(1)-In(2)-N(1) = 101.70(4), O(1)-In(2)-C(11) = 147.31(4), C(11)-In(2)-N(1) = 110.60(6)], whereas both chloride atoms occupy axial sites [Cl(1)-In(2)-Cl(2) = 161.132(13)]. It is most likely the large steric bulk of the ferrocenyl ligand which led to the structural distortion in the equatorial sites.

The observed bonding of In(1) to two ferrocenyl ligands provided insight that indium is capable of bonding to two ferrocenyl ligands, which is required in the target indium complex. In a final attempt to achieve this structural motif, FcLi and $InCl_3$ were reacted in a 2:1 ratio without the

addition of pyridine to ensure that all potential and nonessential steric hindrances were removed and to promote bonding between indium and both ferrocenyl equivalents.

3.3.3 Attempted synthesis of $InFc_2Cl$

The salt elimination reaction of FcLi and indium(III) chloride in toluene was attempted in the absence of pyridine **(Scheme 6)**. The pale-orange solution was cloudy initially but became a clear red/brown solution after a three-hour reaction time. The solution was filtered and concentrated. No evidence of crystallisation occurred when the reaction solution was left at 23 °C in a dinitrogen atmosphere for three days. The solution was further concentrated to 1 mL and stored at -15 °C to induce crystallization. Still, no crystallization or precipitation of product occurred. This prompted the investigation of other solvents which would allow for crystallization to occur. Crystallization attempts from saturated solutions of n-hexane, diethyl ether and THF were unsuccessful. Layering techniques were attempted using diethyl ether/THF and n-hexane/THF in a 3:1 ratio, respectively. The n-hexane/THF solution was stored at -15 °C, where the product separated from the solution as an oil.

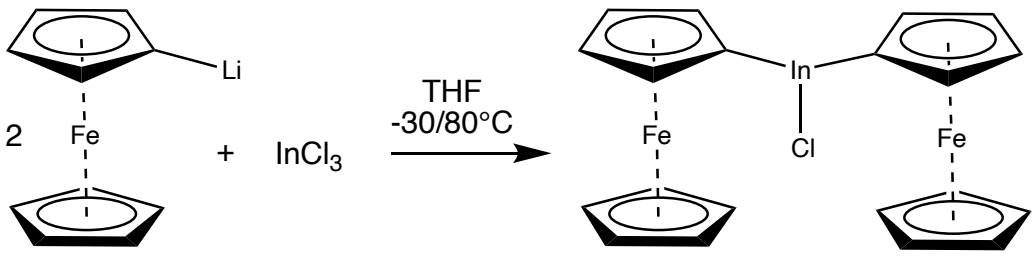

Scheme 6. Proposed synthesis of $InFc_2Cl$ via a salt elimination reaction.

In a final attempt to induce crystallization, the salt elimination reaction was completed as shown in **Scheme 6** and the LiCl salt was removed by filtration before a full molar equivalent of pyridine was added. The clear burnt orange solution became a cloudy brown/orange solution and was concentrated and left at 23 °C for two days. However, no evidence of crystalline material or precipitate was observed. A second equivalent of pyridine was added but the product still did not crystallize or precipitate from solution. When the solution was then stored at -15 °C, a microcrystalline material was observed. The ^{1}H NMR spectrum of the product confirmed the ratio of pyridine and ferrocene to be 1:2, respectively **(Figure A.14)**. This was characteristic of the target complex and thus the crystals were sent for X-ray crystallography. However, the sample degraded during shipping and the remaining sample was very fine particulate matter that could not be characterized through X-ray crystallography. Thus, this reaction route to synthesizing the target complex was abandoned because of the inability to induce crystallization and confirm the identity of the product.

3.4 Reactivity and Computational Studies of Complexes 1 and 2

3.4.1 Reactivity of $InFcCl_2(py)_2$ (1) with I_2

To explore the reactivity of **1**, the complex was reacted I_2, a mild oxidizing agent **(Scheme 7)**. The dark purple solution of I_2 was added dropwise to a clear orange solution of **1**, resulting in an immediate colour change to a dark brown solution. The reaction was stirred for four hours to afford a green muddy colored solution. The solution was filtered to give an amber-brown saturated solution and a small amount of white precipitate. The filtrate was stored at 23 °C for three days to yield colourless needle-like microcrystals in an orange solution. However, this crystalline material was not suitable for X-ray crystallography. Therefore, re-crystallization

attempts were completed in various polar solvents with the aim of increasing the size of the crystals. The product was insoluble in dichloromethane (DCM), acetonitrile and toluene; thus, the re-crystallization attempts were unsuccessful.

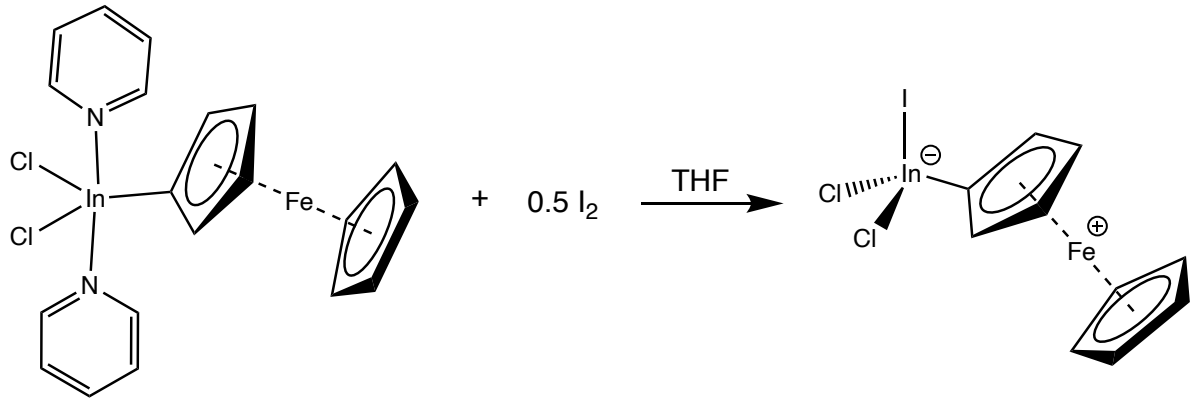

Scheme 7. Addition of **1** to a solution of I_2 in THF to afford the proposed product ($InFcCl_2I$).

A ^1H NMR spectrum of the product was obtained **(Figure A.8)** where an upfield shift of the ferrocenyl peak relative to complex **1** was observed. There was also a significant difference in the ratio of pyridine to ferrocenyl ligand, which suggests that the I_2 reaction led to the displacement of both pyridine ligands as only residual amounts of pyridine are visible in the ^1H NMR spectrum. These preliminary spectroscopic results, along with the observed color change from orange to colorless crystals, suggest that a reaction occurred between **1** and I_2. The proposed product is the zwitterion $InFcCl_2I$. However, further studies are required to confirm the identity of the product.

DFT calculations were performed to provide insight into the reactivity of complex **1** with I_2. The HOMO (Highest Occupied Molecular Orbital) of **1** is shown in **Figure 10**, which indicates that it is located on the ferrocenyl ligand. This suggests that the reaction of complex **1** with I_2 involves the oxidation of the ferrocenyl ligand to the ferrocenium ion.

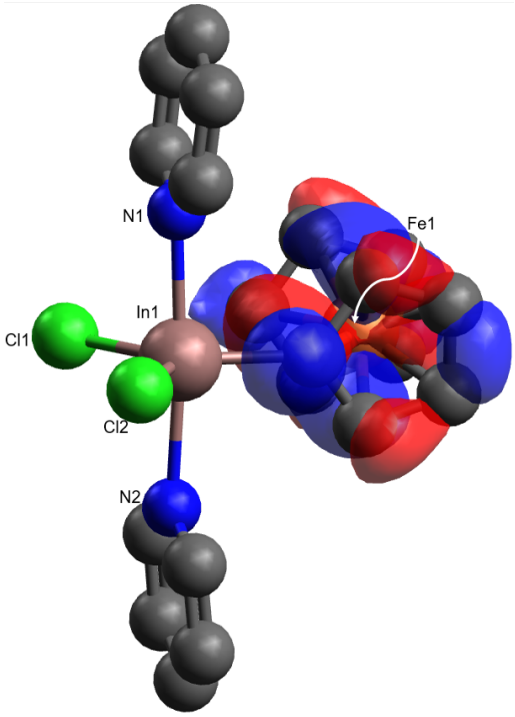

Figure 10. The calculated HOMO of complex **1** where all hydrogens are omitted for clarity.

3.4.2 Reactivity of $In_3Fc_4(py)_2Cl_3O$ (2) with I_2

The reactivity of complex **2** with the I_2 oxidizing agent was also explored **(Scheme 8)**. A dark purple solution of I_2 was added dropwise to a cloudy orange solution of **2**, resulting in an immediate colour change to an opaque brown solution. Half molar equivalents of I_2 were added hourly until a total of 2 molar equivalents were added to the reaction mixture. No further visible colour changes were observed during the four-hour reaction time, though a small green tint was observed in the top layer of solution following the reaction. The dark brown solution was filtered to afford a clear, brown-green solution and a very small amount of brown precipitate. The filtrate was concentrated under vacuum to afford a much darker brown solution. This was stored at 23 °C for three days to form colorless needle microcrystals in an amber solution. Re-crystallization

attempts using DCM, acetonitrile, and toluene were unsuccessful and X-ray crystallography could not be completed on the crystalline material.

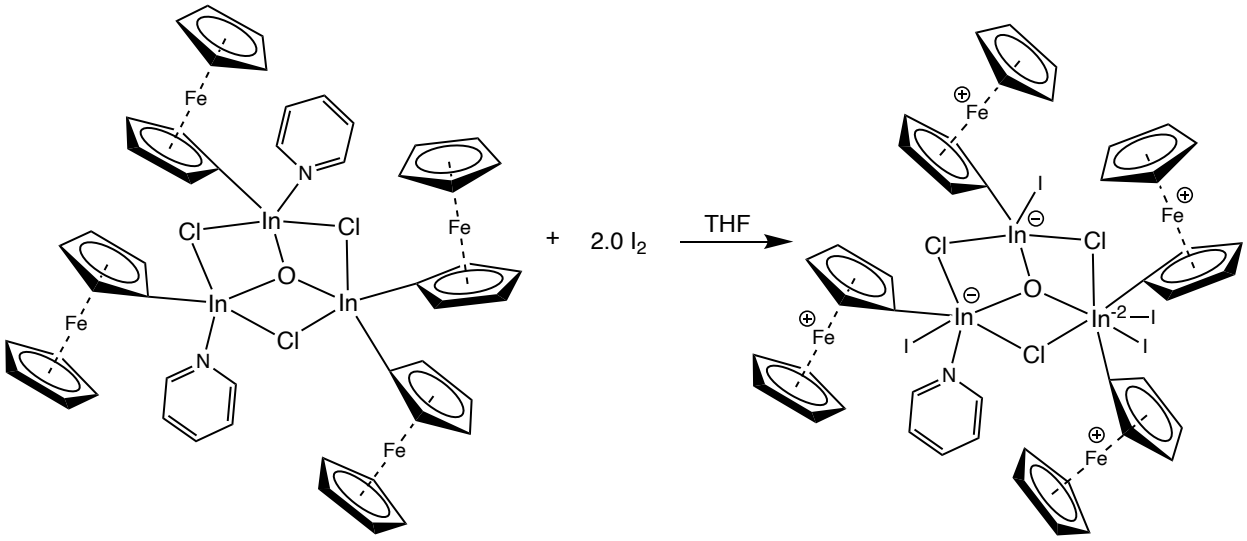

Scheme 8. Addition of complex **2** to a solution of I_2 in THF to afford the proposed product $In_3Fc_4Cl_3O(py)$.

^{1}H NMR data were collected **(Figure A.9)** to propose a structure of the reaction product. Again, a slight upfield shift of the ferrocenyl ligand peak was observed as it oxidized to become ferrocenium ions. The integration values also suggest that a pyridine ligand was displaced from one of the In(2) centres as a 4:1 ratio of ferrocenium ion to pyridine peaks was observed. Based on the observed differences in the ^{1}H NMR spectra and the obvious colour change from orange to colorless crystals, it can be concluded that an oxidation reaction of complex **2** with I_2 occurred. Further studies are required to confirm these preliminary results and ultimately, the final structure of the complex. DFT calculations were also completed to provide insight into the reactivity of complex **2** with I_2. The HOMO of complex **2 (Figure 11)** is located on both $InFc_2$ ferrocenyl ligands. This suggests the oxidation reaction with I_2 will occur at the $In(Fc)_2$ ferrocenyl ligands before the InFc(py) ferrocenyl ligands.

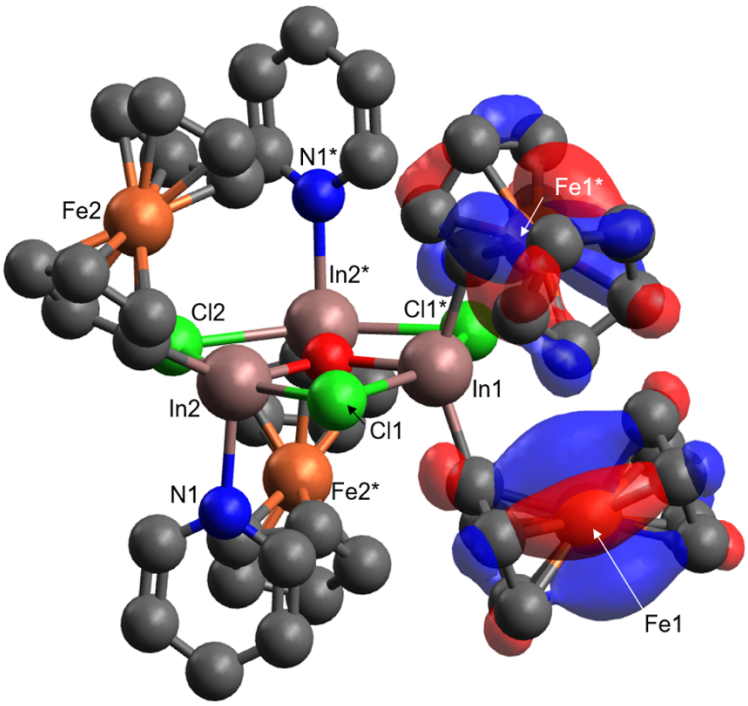

Figure 11. The calculated HOMO of complex **2** where all hydrogens are omitted for clarity.

3.5 Electrochemical Studies of Complexes 1 and 2

The redox properties of both complex **1** and complex **2** were examined via cyclic voltammetry (CV). The CV trace of complex **1** closely resembles that of ferrocene, where a reversible one-electron oxidation wave is observed **(Figure 12)**. These data suggest the structure of **1** remains intact throughout the oxidation and reduction processes. The half-wave potential of **1** (+0.042 V) is very slightly lower than that of ferrocene (+0.081 V). The computational studies of neutral compound **1** shows that the HOMO is centered on the ferrocenyl ligand **(Figure 10)**. This suggests that the electrochemical oxidation involves the oxidation of the ferrocenyl ligand to the ferrocenium ion.

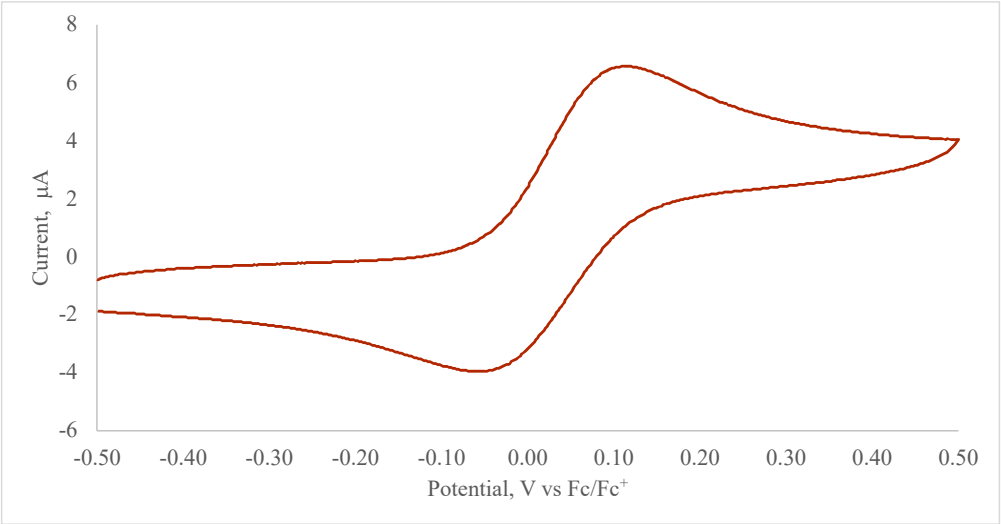

Figure 12. Cyclic voltammogram for compound **1** (1 mM in CH_3CN/0.1 M Bu_4NPF_6, platinum disk electrode, 100 mV/sec).

The CV trace of complex **2 (Figure 13)** is much more complicated than that of compound **1**. The indium trimer contains four ferrocenyl ligands in two different chemical environments. Two ferrocenyl ligands are attached to separate InFc(py) centres and two are attached to the same $InFc_2$ centre **(Scheme 8)**. All four ferrocenyl iron centres are expected to undergo oxidation. The CV trace shows four oxidation peaks and two reduction peaks. Computational studies of neutral compound **2** shows that the HOMO is centred on both $InFc_2$ ferrocenyl ligands, as shown in **Figure 11**. This suggests that the $InFc_2$ ferrocenyl ligands oxidize at lower potential, followed by both InFc(py) ferrocenyl ligands. Further computational studies are required to confirm the sequence of these oxidation steps, as well as the observed reduction steps.

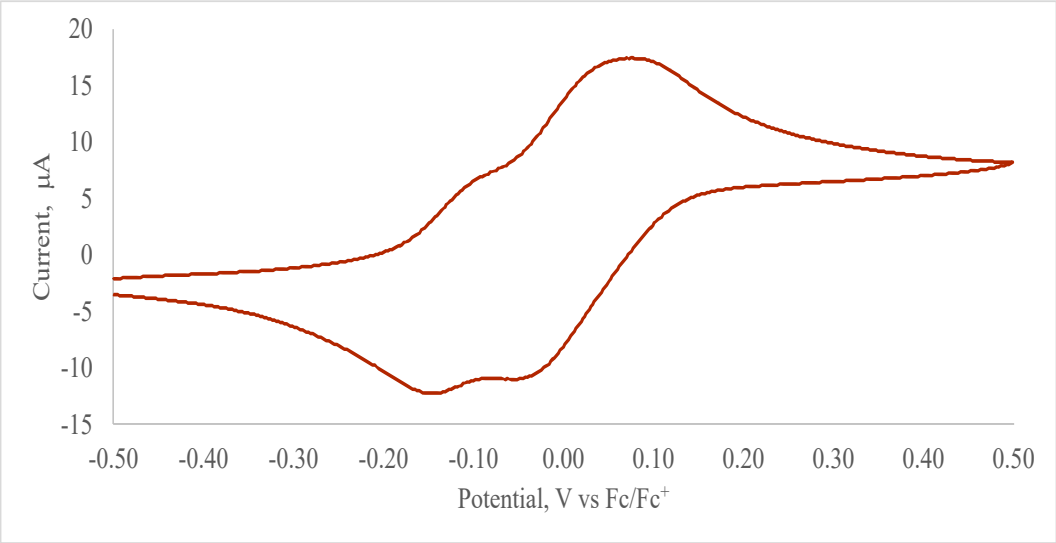

Figure 13. Cyclic voltammogram for compound **2** (1 mM in CH_3CN/0.1 M Bu_4NPF_6, platinum disk electrode, 100 mV/sec).

4. Conclusions

The purpose of this study was to synthesize, characterize and assess the chemical and electrochemical reactivity of indium ferrocene complexes as potential catalytic alternatives. In conclusion, a reproducible and small-scale synthesis of the FcLi ligand was established. A reproducible procedure to synthesize $InFcCl_2(py)_2$ **(1)** as orange block-like crystals was also established, and the structure was confirmed through X-ray crystallography. An unprecedented indium trimer with a central oxo ligand was synthesized $[In_3Fc_4Cl_3O(py)_2]$ **(2)** and confirmed by X-ray crystallography. Full characterization (^{1}H NMR, $^{13}C\{^1H\}$ NMR, FT-IR spectroscopy, melting point, and elemental analysis) of **1** and **2** were completed.

The chemical and electrochemical oxidation of **1** and **2** was explored to assess their reactivity. Both complexes were oxidized when reacted with I_2. Both complexes also exhibited electrochemically reversible redox activity; complex **1** undergoes a one-electron reversible redox process while the CV trace of complex **2** indicates at least two oxidation reactions and two reduction reactions occurred.

5. Future Research

In the future, this research can be continued by exploring new synthetic routes to obtain the target indium ferrocenyl complex [$InFc_2Cl(py)_2$]. More work is needed to confirm and characterize both products obtained from the reaction of **1** and **2** with I_2. Electron paramagnetic resonance spectroscopy can provide further structural information of the zwitterionic products of **1** and **2** with I_2. The reactivity scope of both complexes **1** and **2** could be expanded by reacting them with more oxidants, such as dioxygen and diphenyl disulfide. Theoretical calculations should be completed on **1** and **2** to better interpret the electrochemical results.

6. References

(1) Broughton, E. The Bhopal Disaster and Its Aftermath: A Review. *Environmental Health* **2005**, *4* (1), 6. https://doi.org/10.1186/1476-069X-4-6.

(2) Metzger, J. O. Book Review: Chemistry a Threat?: Green Chemistry. Designing Chemistry for the Environment. Edited by P. T. Anastas and T. C. Williamson. *Angewandte Chemie International Edition in English* **1997**, *36* (7), 783–784. https://doi.org/10.1002/anie.199707831.

(3) Anastas, P. T.; Heine, L. G.; Williamson, T. C. Green Chemical Syntheses and Processes: Introduction. In *Green Chemical Syntheses and Processes*; ACS Symposium Series; American Chemical Society, 2000; Vol. 767, pp 1–6. https://doi.org/10.1021/bk-2000-0767.ch001.

(4) Anastas, P.; Eghbali, N. Green Chemistry: Principles and Practice. *Chemical Society Reviews* **2010**, *39* (1), 301–312. https://doi.org/10.1039/B918763B.

(5) Cue, B. W.; Zhang, J. Green Process Chemistry in the Pharmaceutical Industry. *Green Chemistry Letters and Reviews* **2009**, *2* (4), 193–211. https://doi.org/10.1080/17518250903258150.

(6) Betts, K. *How Industrial Applications in Green Chemistry Are Changing Our World*; American Chemical Society, 2015.

(7) Hollmann, F.; Opperman, D. J.; Paul, C. E. Biocatalytic Reduction Reactions from a Chemist's Perspective. *Angewandte Chemie International Edition* **2021**, *60* (11), 5644–5665. https://doi.org/10.1002/anie.202001876.

(8) Delidovich, I.; Palkovits, R. Catalytic versus Stoichiometric Reagents as a Key Concept for Green Chemistry. *Green Chem.* **2016**, *18* (3), 590–593. https://doi.org/10.1039/C5GC90070K.

(9) Sheldon, R.; Arends, I.; Hanefeld, U. *Green Chemistry and Catalysis*; Wiley-VCH: Weinheim, 2007.

(10) Anastas, P. T.; Kirchhoff, M. M.; Williamson, T. C. Catalysis as a Foundational Pillar of Green Chemistry. *Applied Catalysis A: General* **2001**, *221* (1), 3–13. https://doi.org/10.1016/S0926-860X(01)00793-1.

(11) *Transition-Metal Catalyzed Modification of Nucleosides - ScienceDirect*. https://www.sciencedirect.com/science/article/pii/B9780128112922000064 (accessed 2022-10-13).

(12) Gusevskaya, E. V. Organometallic Catalysis: Some Contributions to Organic Synthesis. *Quím. Nova* **2003**, *26*, 242–248. https://doi.org/10.1590/S0100-40422003000200017.

(13) Praneeth, V. K. K.; Ringenberg, M. R.; Ward, T. R. Redox-Active Ligands in Catalysis. *Angewandte Chemie International Edition* **2012**, *51* (41), 10228–10234. https://doi.org/10.1002/anie.201204100.

(14) Chirik, P. J.; Wieghardt, K. Radical Ligands Confer Nobility on Base-Metal Catalysts. *Science* **2010**, *327* (5967), 794–795. https://doi.org/10.1126/science.1183281.

(15) Shen, Z.-L.; Wang, S.-Y.; Chok, Y.-K.; Xu, Y.-H.; Loh, T.-P. Organoindium Reagents: The Preparation and Application in Organic Synthesis. *Chem. Rev.* **2013**, *113* (1), 271–401. https://doi.org/10.1021/cr300051y.

(16) Schneider, U.; Kobayashi, S. Low-Oxidation State Indium-Catalyzed C–C Bond Formation. *Acc. Chem. Res.* **2012**, *45* (8), 1331–1344. https://doi.org/10.1021/ar300008t.

(17) Sestelo, J. P.; Sarandeses, L. A.; Martínez, M. M.; Alonso-Marañón, L. Indium(III) as π-Acid Catalyst for the Electrophilic Activation of Carbon–Carbon Unsaturated Systems. *Org. Biomol. Chem.* **2018**, *16* (32), 5733–5747. https://doi.org/10.1039/C8OB01426D.
(18) Chauhan, K. K.; Frost, C. G. Advances in Indium-Catalysed Organic Synthesis. *J. Chem. Soc., Perkin Trans. 1* **2000**, No. 18, 3015–3019. https://doi.org/10.1039/A906657H.
(19) Douglas, A. F.; Patrick, B. O.; Mehrkhodavandi, P. A Highly Active Chiral Indium Catalyst for Living Lactide Polymerization. *Angewandte Chemie International Edition* **2008**, *47* (12), 2290–2293. https://doi.org/10.1002/anie.200705033.
(20) Jung, H. J. Neutral and Cationic Indium Complexes for the Synthesis of Functionalized Monomers and Polymers, University of British Columbia, 2022. https://doi.org/10.14288/1.0416491.
(21) Bardají, M.; Coco, S. 14.09 - Organometallic Mesogens. In *Comprehensive Organometallic Chemistry IV*; Parkin, G., Meyer, K., O'hare, D., Eds.; Elsevier: Oxford, 2022; pp 285–338. https://doi.org/10.1016/B978-0-12-820206-7.00119-0.
(22) Obuah, C.; K. Ainooson, M.; Darkwa, J. Effects of Electrochemical Properties of Ferrocenylpyrazolylnickel(Ii) and Palladium(Ii) Compounds on Their Catalytic Activities in Ethylene Oligomerisation Reactions. *RSC Advances* **2018**, *8* (10), 5362–5371. https://doi.org/10.1039/C7RA13588B.
(23) *Ferrocenes: Ligands, Materials and Biomolecules*; Stepnicka, P., Ed.; Wiley, 2008.
(24) Torriero, A. A. J.; Shiddiky, M. J. A.; Burgar, I.; Bond, A. M. Homogeneous Electron-Transfer Reaction between Electrochemically Generated Ferrocenium Ions and Amine-Containing Compounds. *Organometallics* **2013**, *32* (20), 5731–5739. https://doi.org/10.1021/om4002318.
(25) Fedushkin, I. L.; Dodonov, V. A.; Skatova, A. A.; Sokolov, V. G.; Piskunov, A. V.; Fukin, G. K. Redox-Active Ligand-Assisted Two-Electron Oxidative Addition to Gallium(II). *Chemistry – A European Journal* **2018**, *24* (8), 1877–1889. https://doi.org/10.1002/chem.201704128.
(26) R. Luca, O.; H. Crabtree, R. Redox-Active Ligands in Catalysis. *Chemical Society Reviews* **2013**, *42* (4), 1440–1459. https://doi.org/10.1039/C2CS35228A.
(27) Schachner, J. A.; Orlowski, G. A.; Quail, J. W.; Kraatz, H.-B.; Müller, J. Synthesis, Characterization, and Electrochemical Studies on [1.1]Ferrocenophanes Containing Aluminum, Gallium, and Indium. *Inorg. Chem.* **2006**, *45* (1), 454–459. https://doi.org/10.1021/ic051616y.
(28) Rebiere, F.; Samuel, O.; Kagan, H. B. A Convenient Method for the Preparation of Monolithioferrocene. *Tetrahedron Letters* **1990**, *31* (21), 3121–3124.
(29) Goldberg, S. I.; Keith, L. H.; Prokopov, T. S. A Convenient Preparation of Monolithioferrocene1. *J. Org. Chem.* **1963**, *28* (3), 850–851. https://doi.org/10.1021/jo01038a502.
(30) Hedberg, F. L.; Rosenberg, H. Reactions of N-Butyllithium with Haloferrocenes as Routes to Lithioferrocene. *Tetrahedron Letters* **1969**, *10* (46), 4011–4012. https://doi.org/10.1016/S0040-4039(01)88600-7.
(31) Seyferth, D.; Hofmann, H. P.; Burton, R.; Helling, J. F. Triphenylgermyl-Substituted Ferrocenes and Related Compounds. New Syntheses of Ferrocenyl Lithium and Grignard Reagents. *Inorganic Chemistry* **1962**, *1* (2), 227–231.

(32) Bildstein, B.; Malaun, M.; Kopacka, H.; Wurst, K.; Mitterbock, M.; Ongania, K.-H.; Opromolla, G.; Zanello, P. N,N'-Diferrocenyl-N-Heterocyclic Carbenes and Their Derivatives. *Organometallics* **1999**, *18* (21), 4325–4336.
(33) Mueller-Westerhoff, U.; Yang, Z.; Ingram, G. A Simple Synthesis of Metallocene Aldehydes from Lithiometallocenes and N, N-Dimethylformamide: Ferrocene and Ruthenocene Aldehydes and 1,1'-Dialdehydes. *Journal of Organometallic Chemistry* **1993**, *463*, 163–167.
(34) Schachner, J. A.; Lund, C. L.; Burgess, I. J.; Quail, J. W.; Schatte, G.; Müller, J. The Dynamic Indium-Bridged [1.1] Ferrocenophane. *Organometallics* **2008**, *27*, 4703–4710.
(35) Buchholz, D. B.; Ma, Q.; Alducin, D.; Ponce, A.; Jose-Yacaman, M.; Khanal, R.; Medvedeva, J. E.; Chang, R. P. H. The Structure and Properties of Amorphous Indium Oxide. *Chem. Mater.* **2014**, *26* (18), 5401–5411. https://doi.org/10.1021/cm502689x.

7. Appendix

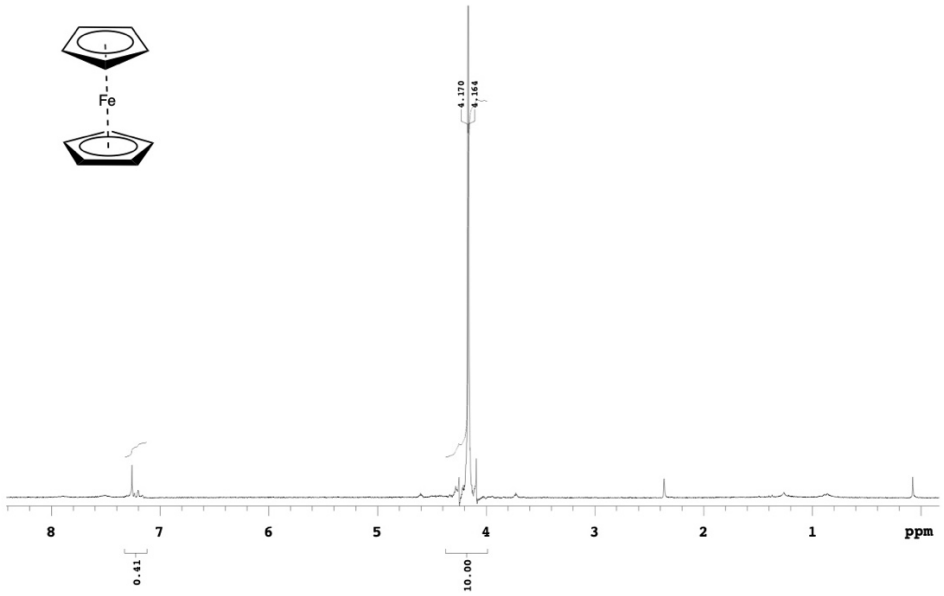

Figure A.1: ^{1}H-NMR spectrum in $CDCl_3$ of the product from the reaction of 2 Fc + 2 tBuLi + $InCl_3$.

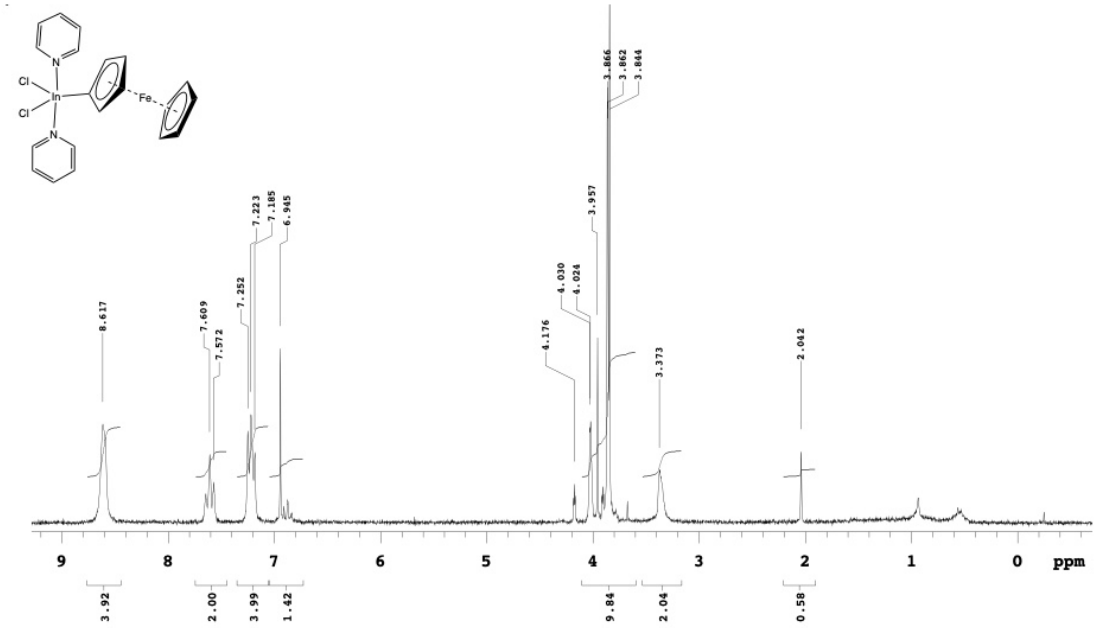

Figure A.2: ^{1}H-NMR spectrum in $CDCl_3$ of $InFcCl_2(py)_2$ **(1)**.

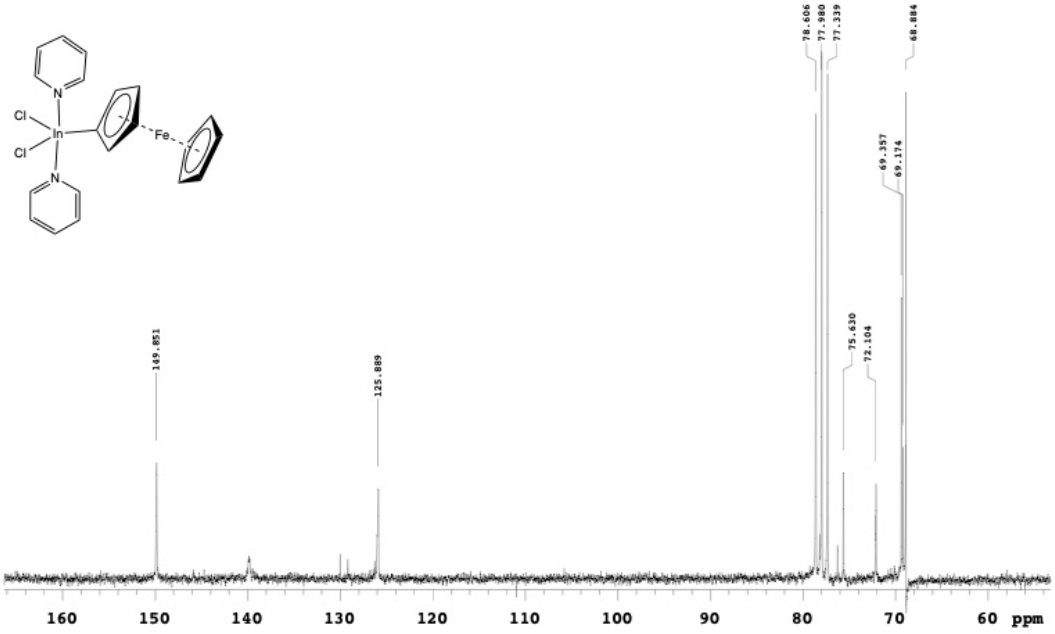

Figure A.3: $^{13}C\{^{1}H\}$-NMR spectrum in $CDCl_3$ of $InFcCl_2(py)_2$ **(1)**.

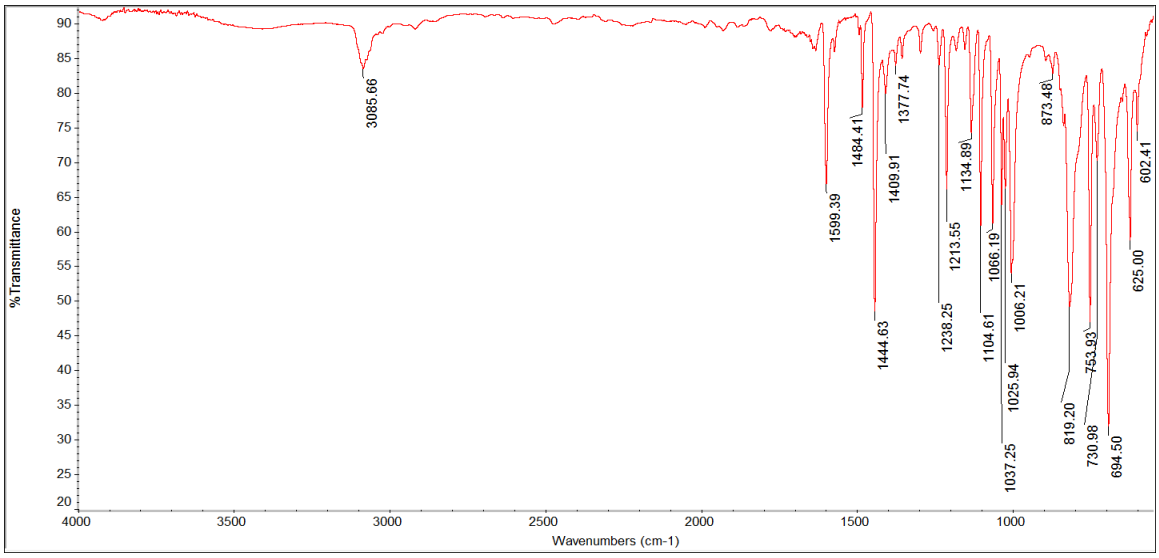

Figure A.4: FT-IR spectrum of $InFcCl_2(py)_2$ **(1)**.

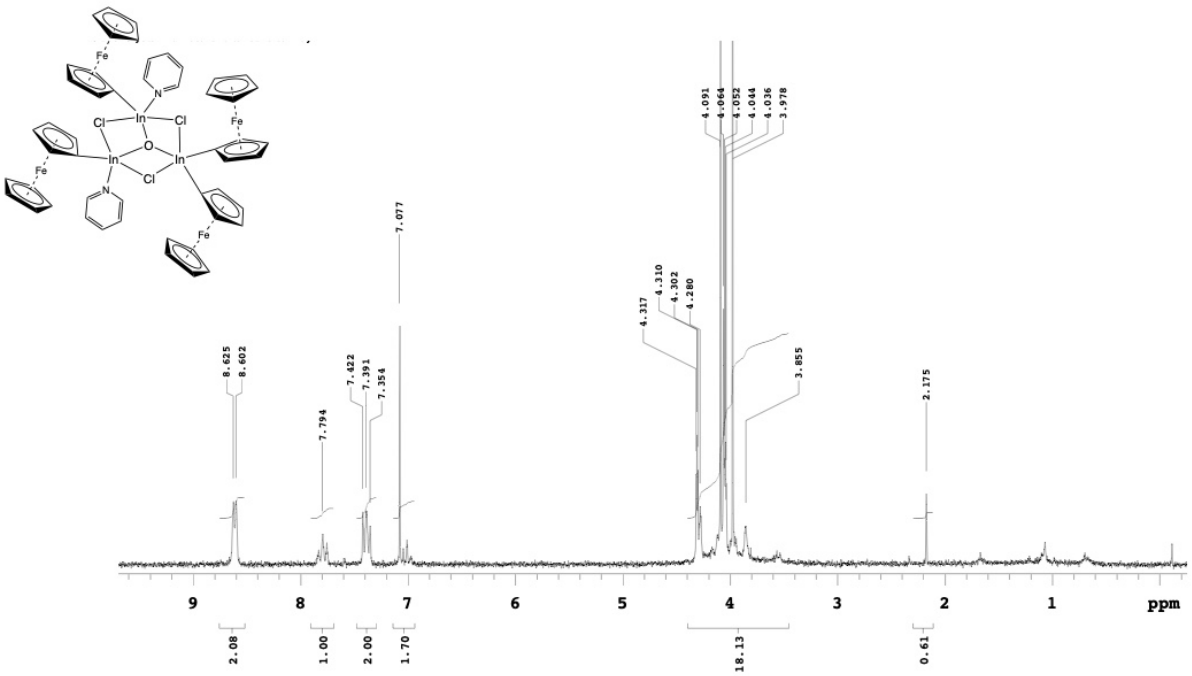

Figure A.5: ^{1}H-NMR spectrum in $CDCl_3$ of $In_3Fc_4Cl_3O(py)_2$ **(2)**.

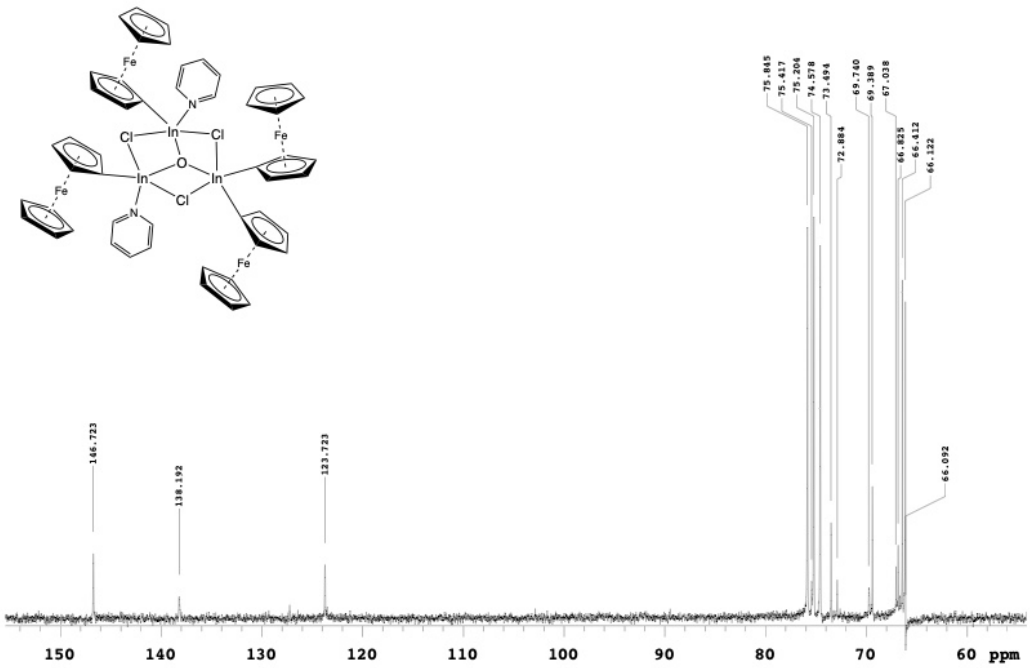

Figure A.6: ^{13}C{^{1}H}-NMR spectrum in $CDCl_3$ of $In_3Fc_4Cl_3O(py)_2$ **(2)**.

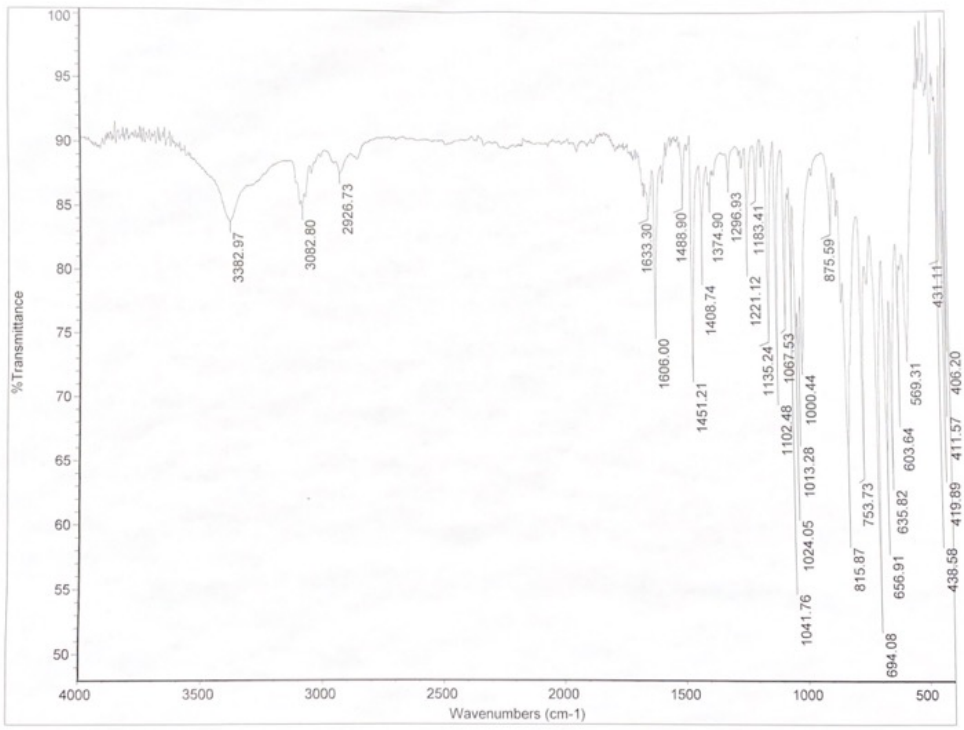

Figure A.7: FT-IR spectrum of $In_3Fc_4Cl_3O(py)_2$ **(2)**.

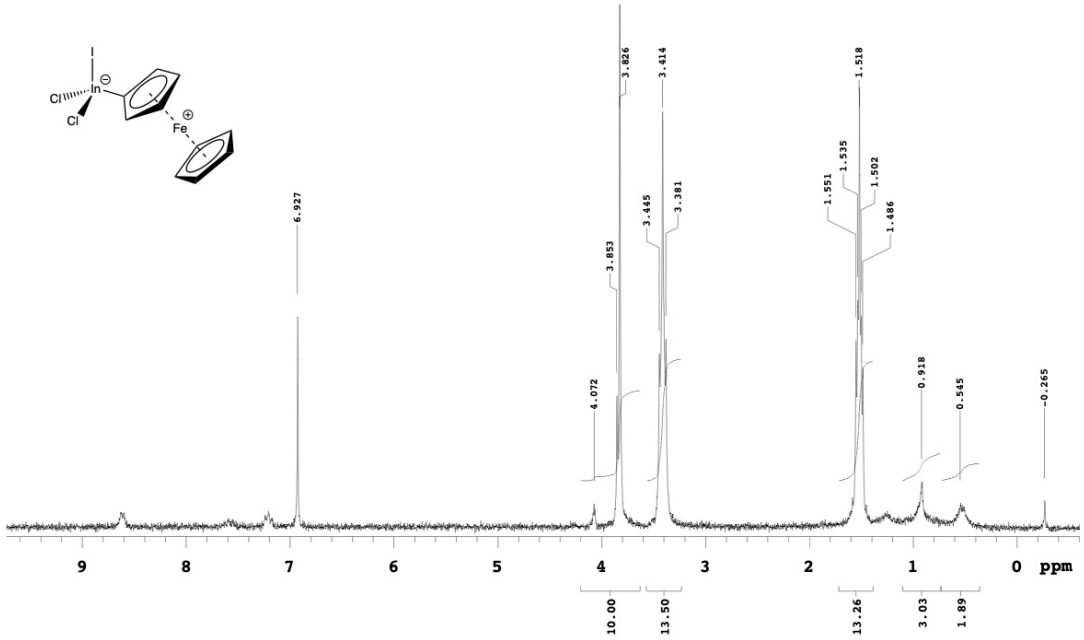

Figure A.8: ^{1}H-NMR spectrum in $CDCl_3$ of $InFcCl_2(py)_2$ **(1)** reaction with I_2.

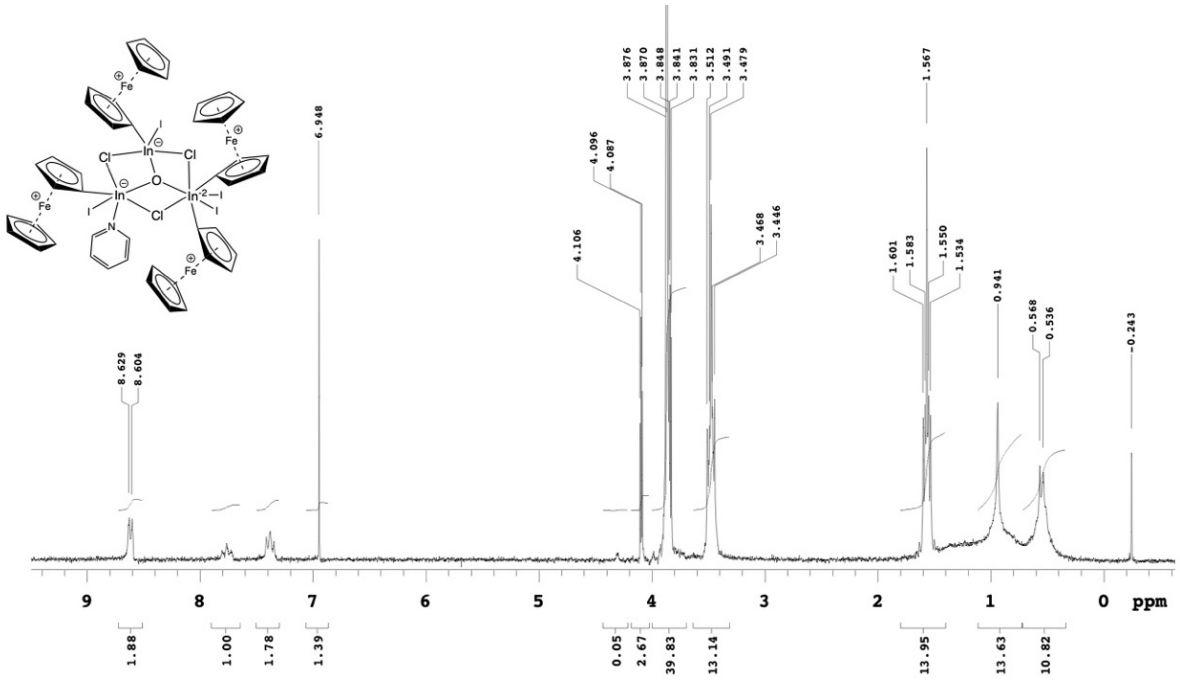

Figure A.9: ^{1}H-NMR spectrum in $CDCl_3$ of $In_3Fc_4Cl_3O(py)_2$ **(2)** reaction with I_2.

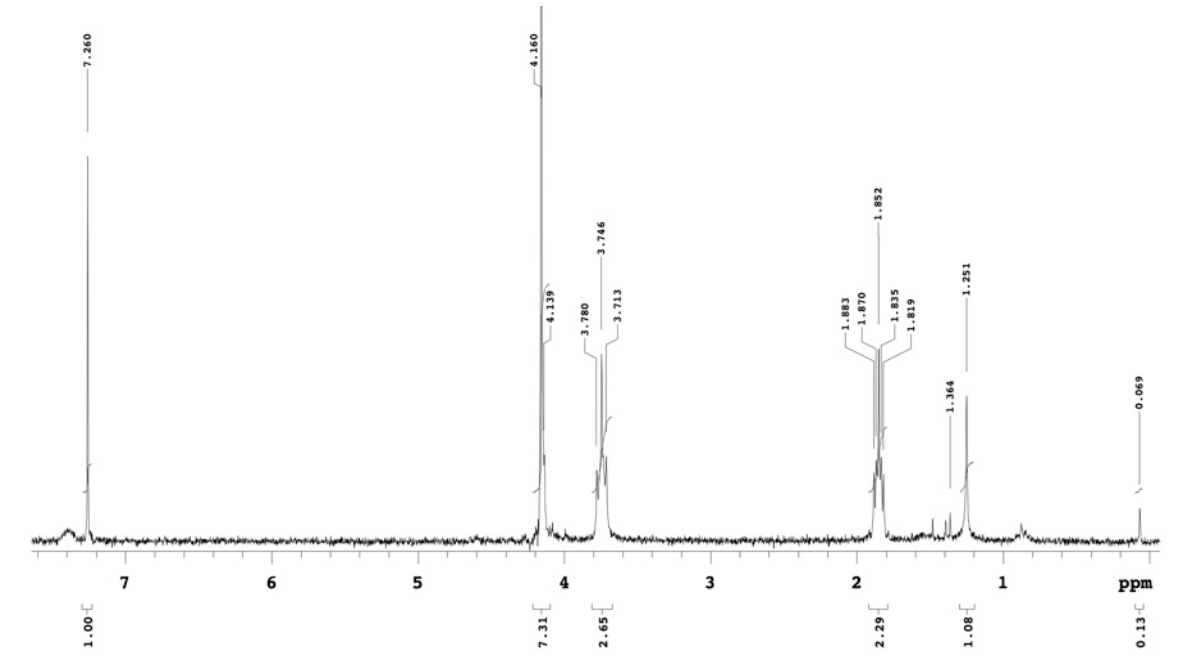

Figure A.10: ^{1}H-NMR spectrum in $CDCl_3$ of the product from the reaction of 2 Fc + 2 tBuLi + $InCl_3$.

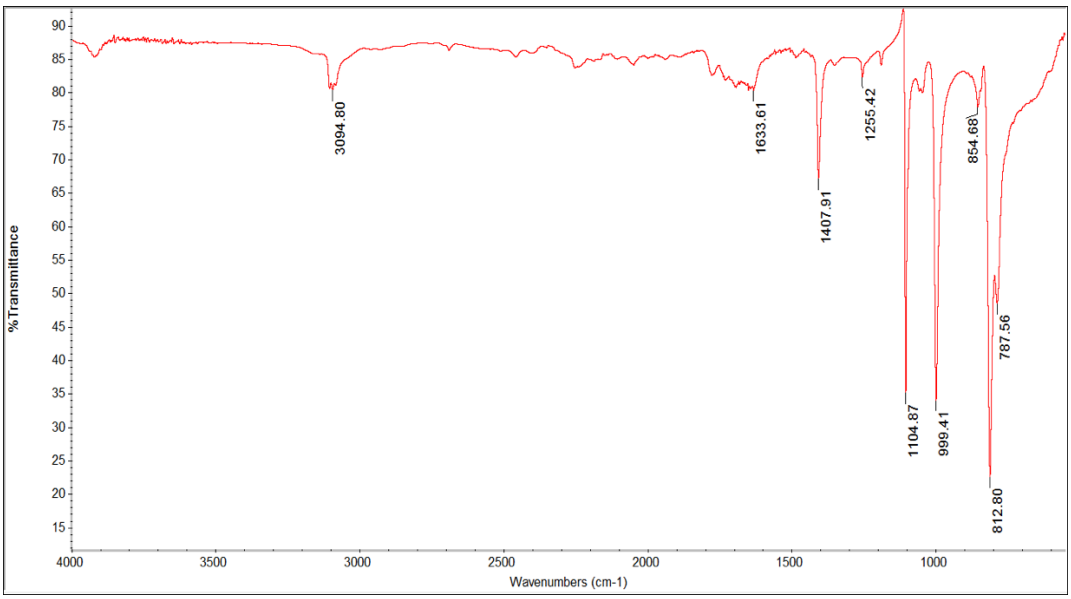

Figure A.11: FT-IR spectra of ferrocene.

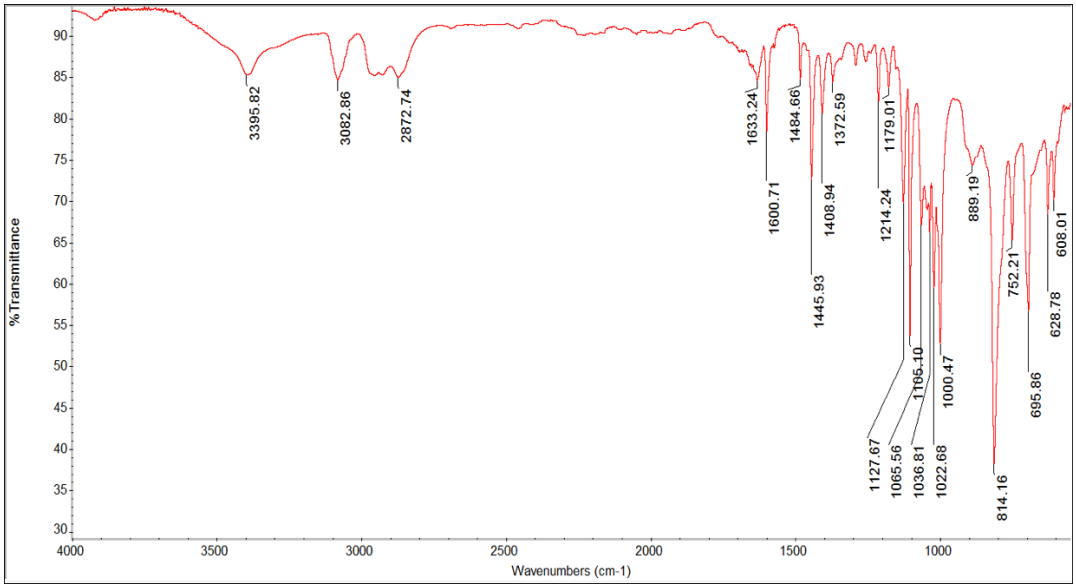

Figure A.12: FT-IR spectrum of the product from the reaction of 2 Fc + tBuLi + $InCl_3$.

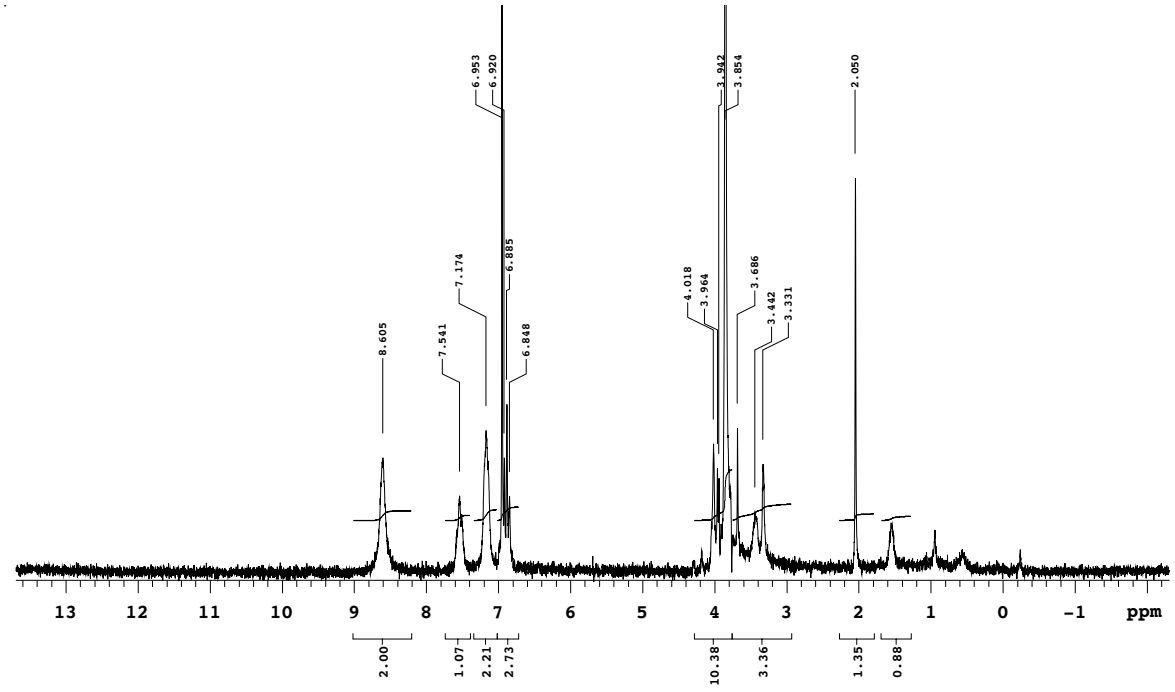

Figure A.13: ^{1}H-NMR spectrum of the product from the reaction of $InCl_3$ + 2 FcLi.